Innovative integrated damping mooring technology for floating wind turbines under extreme sea conditions

Tian, Haonan; Soltani, Mohsen N.; Colomés, Oriol

DOI
10.1016/j.marstruc.2025.103948

Publication date
2025

Document Version
Final published version

Published in
Marine Structures

Marine Structures 106 (2026) 103948

Contents lists available at ScienceDirect

Marine Structures

journal homepage: www.elsevier.com/locate/marstruc

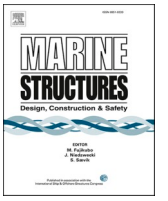

Research Paper

Innovative integrated damping mooring technology for floating wind turbines under extreme sea conditions

Haonan Tian [a,*], Mohsen N. Soltani [a], Oriol Colomés [b]

[a] AAU Energy, Aalborg University, Esbjerg, Denmark
[b] Civil Engineering Department, Technische Universiteit Delft, Netherlands

ARTICLE INFO

Keywords:
Semi-submersible wind turbine
Integrated damping mooring
Ultimate limit state
Safety factor

ABSTRACT

Mooring failures significantly threaten the stability of Floating Offshore Wind Turbines (FOWT) under extreme environmental conditions. This study presents an innovative integrated damping mooring system incorporating Seaflex dampers to improve structural stability and operational reliability. Dynamic simulations under 1-year and 50-year return period sea states demonstrate the system's effectiveness. Under Ultimate Limit State (ULS) conditions, the system reduces surge displacement by 59%, pitch angle by 47%, and mooring line tension by 72%. Under Accidental Limit State (ALS) conditions, it mitigates load spikes, reduces drift displacement by 60%, and improves safety factors by 50%. The comparison shows chain and wire rope configurations have better load reduction performance in the integrated damping scheme. Lightweight and adaptable, the Seaflex dampers enhance broad-spectrum damping without affecting platform buoyancy. This study offers a robust solution for enhancing FOWT safety and durability in harsh marine environments, thereby enabling large-scale offshore wind energy development.

1. Introduction

The Paris Agreement's global emission reduction targets have catalyzed the rapid adoption of renewable energy technologies [1]. According to the International Energy Agency (IEA), floating offshore wind turbines (FOWT) are expected to account for 15–20 % of global offshore wind capacity by 2035, driven by advancements in technology and supportive policies [2]. The Global Wind Energy Council (GWEC) similarly highlights the increasing importance of FOWT in achieving carbon neutrality, particularly in regions with deep-water resources [3]. FOWT can be deployed in waters deeper than 60 m, harnessing stronger and more stable wind resources to achieve higher energy yields [4]. Unlike fixed-bottom turbines, floating platforms avoid seabed disruption, minimizing environmental impact and making them more suitable for deployment in ecologically sensitive marine environments [5]. Also, floating turbines offer greater installation flexibility due to their modular design, simplifying transportation and deployment, which is especially advantageous in remote offshore areas [6]. As technology matures, floating wind energy is poised for significant growth. Larger, more efficient turbines are expected to reduce costs further, making this technology increasingly economically viable.

However, the structural safety of FOWT still faces challenges, particularly regarding mooring systems and floating foundation failures. In the mooring system, transient failure is a critical failure mode, especially under extreme weather conditions such as typhoons and severe storms. Mooring lines may experience transient loads exceeding their design limits, leading to line breakage and causing the FOWT to drift or deviate from its position [7]. Additionally, the violent platform motion caused by wind and waves can

* Corresponding author.
E-mail address: hti@energy.aau.dk (H. Tian).

https://doi.org/10.1016/j.marstruc.2025.103948
Received 9 February 2025; Received in revised form 10 September 2025; Accepted 24 September 2025
Available online 8 October 2025

Nomenclature

M	mass matrix
M_a	added mass matrix
C_{total}	the total equivalen damping matrix
$\xi,\ \dot{\xi},\ \ddot{\xi}$	displacement, velocity and acceleration of floater
k_{h}	hydrostatic restoring stiffness matrix
k_{m}	nonlinear restoring stiffness matrix
$F_{\mathrm{w1}}, F_{\mathrm{w2}}$	first-order and second-order wave excitation force
F_{d}	wind force
$A_j,\ A_k^*$	complex amplitude and its conjugate for the j-th and k-th wave frequency components
ω_j, ω_k	j-th and k-th wave frequency components
L, D	transfer functions for the first order and second order wave forces
E_d	energy dissipation
$m_i,\ a_i$	mass matrix and added mass matrix at mooring node i
$a_{p_i},\ a_{q_i}$	transverse and tangential added mass matrices
$C_L,\ C_d$	lift coefficient and drag cofficient
ρ	air density
ϕ	angle of attack
a	axial induction factor
v_w	velocity of the wind
Δr	blade sections radial length
c	chord length of airfoil
B	blade numbers
d_m	the equivalent mooring line diameter
l	segment length
ρ_m	density of the mooring cable material
I	identity matrix
$C_{\mathrm{an}},\ C_{\mathrm{at}}$	transverse and tangential added mass coefficients
$\widehat{q}_i, \widehat{q}_i^T$	unit tangent direction at node i, and its transpose
F_M	mooring force
$r_i,\ \ddot{r}_i$	position vector at node i, and its acceleration
$T_{i+\frac{1}{2}},\ T_{i-\frac{1}{2}}$	internal tension force
$V_{i+\frac{1}{2}},\ V_{i-\frac{1}{2}}$	cross-sectional shear force
W_i, B_i	lumped weight and net buoyancy at node i
$D_{p_i},\ D_{q_i}$	transverse and tangential directions drag forces
S	transformation operator
l_0	initial length
r_i	nodal position vectors
T	effective force
$p_o,\ p_i$	shear force external and internal pressures
$A_o,\ A_i$	outer and inner cross-sectional areas
E	material stiffness
β	poisson ratio
κ_{tt}	additional terms include torque coupling
θ	twist angle
l_s	segment length
c	damping coefficient
TC_{env}	characteristic environmental tension
T_{MPM}	maximum line tension
T_{pret}	line pretension
s_C	characteristic mooring strength
$\gamma_{\mathrm{pret}}, \gamma_{\mathrm{env}}$	safety factors for pretension and environmental tension
μ	mean of tension time series
σ	standard deviation
T_z	mean up-crossing period
α	probability of exceedance

lead to transient failure of the mooring system, especially in semi-submersible platforms, where severe heave or sway motion may impose additional dynamic loads on the mooring lines and anchors, resulting in instantaneous failure [8]. In some cases, local failures, such as the breakage of a single mooring line, may further trigger system-level failure, potentially causing the collapse of the entire mooring system [9]. To address these risks, classification societies such as DNV have introduced several limit states to evaluate the safety and performance of FOWT under various conditions. The ultimate limit state (ULS) focuses on structural failure due to extreme loading events, such as storms with a 50-year return period. In contrast, the accidental limit state (ALS) assesses the structure's ability to withstand accidental scenarios, such as the failure of a single mooring line, without leading to catastrophic consequences. The definition of these limit states is closely tied to environmental conditions, as they represent the structural and operational thresholds under specific sea states [10].

The ULS and ALS of FOWT are closely tied to environmental conditions, such as wave height, period, and wind speed, which directly influence structural safety and system performance under operational and extreme scenarios [11]. The National Renewable Energy Laboratory (NREL) defines typical sea states for design purposes, such as 1-year and 50-year return periods, which correspond to moderate and extreme conditions, respectively [12]. In a 1-year return period, wave heights are generally moderate, and the associated wave periods are shorter, leading to less intense hydrodynamic loads on the mooring system and floating foundation. These conditions primarily affect the fatigue performance of the mooring lines and structural components, as the system experiences repetitive, sub-critical loading over time [13]. Conversely, in a 50-year return period, wave heights can reach extreme values, often accompanied by long-period waves and sustained high wind speeds. These conditions impose significant dynamic loads on the mooring lines, floating foundation, and tower, which may exceed their design thresholds. Long-period waves amplify platform motions, such as pitch, roll, and heave, increasing the likelihood of mooring line tension spikes and transient failures [14]. The combined effects of extreme wave height, prolonged loading duration, and high wind speeds also challenge the structural stability of FOWT, particularly for semi-submersible platforms and spar-buoy designs, where the interaction between wind and wave loads can induce complex dynamic responses [15]. Moreover, the impact of extreme sea states is not limited to immediate structural integrity. Prolonged exposure to high wind speeds and rough seas during 50-year return conditions can lead to cumulative fatigue damage, significantly shortening the operational life of mooring components and floating foundations [16]. Studies also highlight the potential for local failures, such as a single mooring line breakage, to propagate into system-wide failures under these extreme conditions, especially when coupled with violent platform motions [17]. Understanding the differences between 1-year and 50-year return periods is critical for the safe and cost-effective design of FOWT.

In response to the challenges posed by mooring and floating foundation failures in FOWT, researchers have proposed various strategies to enhance system reliability. These strategies can be broadly categorized into three areas: 1) improvements in mooring designs, 2) advancements in floating foundation structures, and 3) developing mooring damping technologies. Improvements in mooring designs have focused on enhancing load distribution, redundancy, and anchoring techniques to ensure system stability under extreme conditions. Li et al. proposed attaching clump weights and heavy chains to mooring systems to mitigate the impact of extreme weather conditions such as typhoons, effectively reducing load fluctuations and enhancing system stability [18]. Sheng et al. suggested increasing the number of mooring points to distribute forces more evenly, thereby reducing the risk of local failure and improving overall system reliability [19]. To prevent system-wide instability caused by the failure of a single mooring point, van der Giessen et al. introduced a redundant mooring system design, which ensures platform stability even when local anchors fail [20]. Sumer et al. introduced improved anchoring techniques, such as suction and plate anchors, which offer enhanced stability in complex seabed conditions [21]. Reinforcing critical areas of the platform's structure where stress concentrations are the highest has also been proposed to mitigate failure risks.

Advancements in floating foundation structures have aimed at optimizing design and increasing buoyancy to improve stability in harsh sea conditions. Moan et al. highlighted the effectiveness of optimizing floating foundation designs, particularly by using more stable semi-submersible and spar-type structures, which significantly reduce the risk of capsizing during extreme sea conditions [22]. Xu et al. proposed increasing buoyancy structures in floating foundations to enhance platform stability, especially during extreme weather, reducing the likelihood of capsizing [23]. Another innovative approach was discussed by Muskulus and Matha, who examined the interaction between currents, hydrodynamics, and novel foundation technologies, providing new insights into stabilizing FOWT in varying sea conditions [24]. Thomsen et al. (2021) designed the TETRASPAR floating foundation with passive heave plates beneath the structure. These plates increase damping by resisting heave motion, reducing vertical oscillations and stabilizing the platform in challenging sea conditions [25].

As advancements in FOWT continue, the development of mooring damping technologies has emerged as a critical aspect of improving stability and mitigating failure risks. Semyung Park (2020) proposed incorporating tuned liquid column dampers within the floating foundation structure. These systems use liquid movement inside specially designed chambers to counteract platform oscillations. The liquid's inertia helps reduce pitch and roll motions, particularly during storm events [26]. Shape Memory Alloy (SMA) dampers utilize materials that absorb and dissipate energy through their intrinsic phase transition properties. Installed within mooring lines, these dampers provide dynamic damping that adjusts to environmental loads, reducing oscillations and extending the lifespan of the mooring system [27]. Combining catenary and taut mooring lines distributes forces across multiple lines with varying stiffness, reducing peak loads and dynamic responses during storm events. This hybrid system has demonstrated robust performance in FOWT [28]. The Seaflex damper, a flexible viscous damping system designed for underwater use, absorbs energy through its flexible body. Installed along mooring lines, it mitigates dynamic motions caused by waves, reducing strain on the mooring system and enhancing platform stability [29].

These advancements in mooring damping technologies are vital in mitigating dynamic forces and ensuring the long-term reliability of FOWT systems. Among the various technologies, the Seaflex damper stands out due to its distinct advantages. Unlike passive heave

plates or TLCDs, which target specific frequency ranges, the Seaflex damper covers a broad spectrum of load frequencies, making it highly adaptable to varying sea conditions. Additionally, it offers a wide damping range, effectively mitigating dynamic motions across various operational scenarios. Its lightweight design further enhances its practicality, as it does not significantly alter the floating platform's center of mass or buoyancy, unlike bulkier damping systems. These features make the Seaflex damper a particularly effective solution for enhancing the stability of FOWT.

This study proposes an integrated damping mooring system to mitigate the instantaneous impact forces on FOWT. By incorporating Seaflex dampers as intermediate damping units, the study explores the integrated damping effects of connecting ropes of different materials. This study investigates the response of FOWT based on load spectra for extreme wind and wave conditions designed by the international standard IEC 61,400–3–1 [30]. The safety enhancement of this damping technology for mooring systems was evaluated under 1-year and 50-year return period sea states. Additionally, the performance of this technology was compared with other mainstream underwater damping techniques, and its limitations were discussed.

This paper comprehensively examines FOWT mooring systems, covering dynamics modeling, research preparation, case studies, and damping technology comparisons. Section 2 details the FOWT dynamic model and mooring damping model. Section 3 elaborates on the installation schematic and prior results, demonstrating the technology's effectiveness in reducing mooring fatigue damage and extending lifespan under operational sea conditions. Section 4 presents a case study using the NREL 5 MW semi-submersible, simulating its response under 1-year and 50-year return period sea states, comparing system responses and safety factors for ULS and ALS conditions. Section 5 compares mainstream underwater mooring damping technologies. The study concludes by summarizing the characteristics and advantages of the integrated Damping Mooring System, offering engineers a novel approach to enhance wind and wave resistance. The workflow is detailed in Fig. 1.

2. Dynamics model of FOWT

2.1. System dynamics modelling

In the EU OC4 project, the interaction between the floating foundation of the 5MW semi-submersible wind turbine and ocean waves can be described using a mass-spring-damper system based on the Cummins equation. The external loads include the first-order wave excitation force, second-order difference-frequency wave force, and total wind force [31].

$$(M+M_a(\infty))\ddot{\xi}(t)+\int_0^t K(t-\tau)\dot{\xi}(\tau)d\tau+C_v\dot{\xi}(t)+k_{total}\xi(t)=F_{exc}(t) \tag{1}$$

$$F_{exc}(t,\dot{\xi}(t))=F_{w1}(t)+F_{w2}(t)+F_d(t,\dot{\xi}(t)) \tag{2}$$

$$k_{\text{total}}=k_m(\xi(t))+k_h(\xi(t)) \tag{3}$$

In this equation, M is the mass matrix, $M_a(\infty)$ is the added mass matrix at infinite frequency, and C_{total} combines potential radiation damping and equivalent linearized viscous, all sized 6×6. $K(t)$ denotes the radiation damping memory function. It is calculated based on potential flow theory, reflecting the fluid memory effect. C_v represents the equivalent linearized viscous damping coefficient, reflecting the viscous dissipation effect. k_{h} is the hydrostatic restoring stiffness matrix, k_{m} is the nonlinear restoring stiffness matrix from the mooring system. This study only introduces roll-direction equivalent linear damping, set at 5 % of critical damping [23]. The $\xi(t)$ represents the displacement of the floating body in six degrees of freedom. The vectors $\ddot{\xi}(t)$ and $\dot{\xi}(t)$ denote the accelerations and

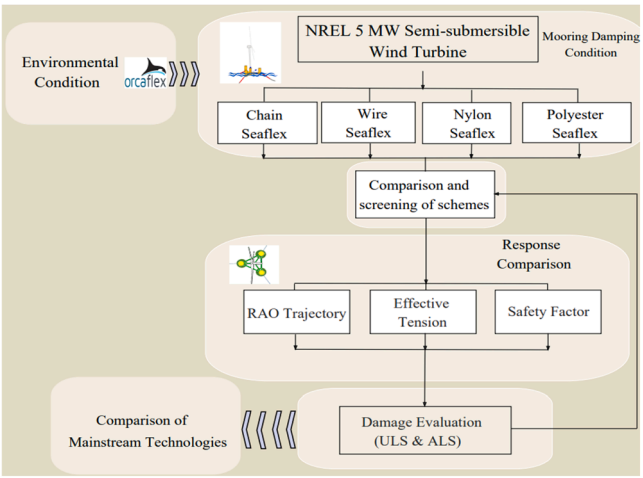

Fig. 1. Article flowchart.

velocities in the six degrees of freedom. Here, $F_{w1}(t), F_{w2}(t)$, and F_d represent the first-order wave excitation force, second-order difference-frequency wave force, and total wind force, as seen in Eqs. (4) to (6).

$$F_{w1}(t) = \mathrm{Re}\left(\sum_{j=1}^{Nw} A_j L(\omega_j) e^{i\omega j t}\right) \tag{4}$$

$$F_{w2}(t) = \mathrm{Re}\left(\sum_{j=1}^{Nw}\sum_{k=1}^{Nw} A_j A_k^* D(\omega_j, \omega_k) e^{i(\omega_j - \omega_k)t}\right) \tag{5}$$

$$F_d = \frac{1}{2}(C_L\cos\phi + C_d\sin\phi)\rho {v_w}^2(1-a)^2 cB\frac{\Delta r}{\sin^2\phi} \tag{6}$$

In the equations above, the parameters are defined as follows: A_j and A_k^* represent the complex amplitude and its conjugate for the j-th and k-th wave frequency components, while ω_j and ω_k denote their respective frequencies, with N_w as the total number of wave components. $L(\omega_j)$ and $D(\omega_j, \omega_k)$ are the transfer functions for the first order and second order wave forces, respectively. In the aerodymic thrust function, where C_L is the lift coefficient, C_d is the drag coefficient; ρ is the air density; v_w is the velocity of the wind; ϕ is the angle of attack; a is the axial induction factor; Δr is the blade sections radial length; c is the chord length of airfoil and B is the blade numbers.

2.2. Dynamic characteristics of integrated damping mooring

To further analyze the mooring dynamics with integrated damping as shown in the Fig. 2, we constructed the FOWT system in OrcaFlex software. This software is developed for the hydrodynamic and mooring dynamics components of the OC4 project. These mooring lines are divided into numerous massless segments, each with specific stiffness characteristics, while the mass is concentrated at the nodes. The response of the moored mass points is mainly influenced by multiple factors, including internal axial stiffness, damping forces, buoyancy, and hydrodynamic forces described by Morison's equation. A finite element model of the mooring line was established in Orcaflex to simulate this dynamic process numerically [33]. The mooring line, approximately 835.5 m in length, was discretised into 84 nodes, with the parameters of the line segments, including mass, weight, and buoyancy, lumped at these nodes to simplify the calculations.

$$F_M = \sum_{i=1}^{N}(m_i + a_i)\ddot{r}_i = S\sum_{i=1}^{N}\left(T_{i+\left(\frac{1}{2}\right)} - T_{i-\left(\frac{1}{2}\right)} + V_{i+\left(\frac{1}{2}\right)} - V_{i-\left(\frac{1}{2}\right)} + W_i + B_i + D_{pi} + D_{qi} + F_{s\_i}\right) \tag{7}$$

$$m_i = \frac{\pi}{4}{d_m}^2 l\rho I \tag{8}$$

$$a_i = a_{pi} + a_{qi} = \rho_m\frac{\pi}{4}{d_m}^2 l\left[C_{an}\left(I - \hat{q}_i\hat{q}_i^T\right) + C_{at}\left(\hat{q}_i\hat{q}_i^T\right)\right] \tag{9}$$

Among these parameters, m_i denotes the mass matrix at mooring node i; a_i represents the added mass matrix at mooring node i, composed of the transverse (a_{p_i}) and tangential (a_{q_i}) added mass matrices; d_m is the equivalent mooring line diameter; l is the segment length; ρ_m is the density of the mooring cable material; I is the identity matrix; C_{an} and C_{at} are the transverse and tangential added mass coefficients, respectively; $\hat{q}_i$ is the unit tangent direction at node i, and $\hat{q}_i^T$ is its transpose; F_M is the mass-related force term (representing the inertial forces that include both mass and added-mass effects); r_i is the position vector at node i, and $\ddot{r}_i$ is its acceleration; N is the total number of nodes; $T_{i+\frac{1}{2}}$ and $T_{i-\frac{1}{2}}$ are the internal tensions contributed by the segments adjacent to node i; $V_{i+\frac{1}{2}}$ and $V_{i-\frac{1}{2}}$ are the cross-sectional shear forces of those segments; W_i is the lumped weight at node i; B_i is the net buoyancy at node i; D_{p_i} and D_{q_i} are the

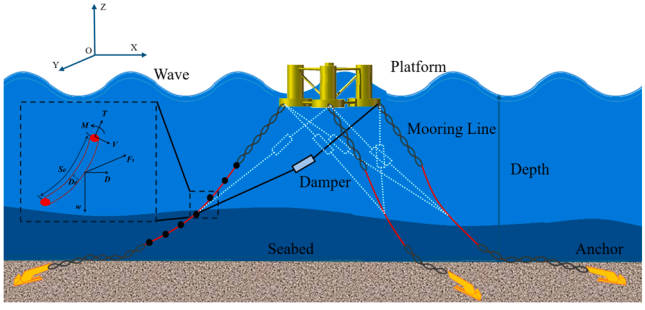

Fig. 2. The connection scheme of the integrated damping mooring system.

drag forces acting in the transverse and tangential directions at node i, respectively; and S is a transformation operator (used for coordinate transformations).

For the line segment connecting nodes i and $i+1$, its length $l(t)$ and the initial length l_0 determine the strain ε and the strain rate $\frac{dl}{dt}$ as follows:

$$\varepsilon(t) = \frac{l(t) - l_0}{l_0}, \quad \frac{dl}{dt} = \frac{d}{dt}[l_0(1+\varepsilon)] = l_0 \frac{d\varepsilon}{dt} \tag{10}$$

In numerical analyses, $\varepsilon(t)$ and $\frac{dl}{dt}$ can be obtained based on the time-dependent variation of the nodal position vectors $r_i(t)$. By substituting the strain and strain rate into the line segment tension equations, the internal axial tension within the segment can be determined. During this process, various factors are considered. These include the material's elastic properties, such as Young's modulus and cross-sectional area. They also encompass pressure differentials, both external and internal, along with their corresponding cross-sectional areas.

The following equations give the effective tension and shear force in the mooring lines:

$$T = V + (p_o A_o - p_i A_i) \tag{11}$$

$$V = EA_{\mathrm{m}}\varepsilon - 2\beta(p_o A_o - p_i A_i) + \kappa_{\mathrm{tt}}\frac{\theta}{l_s} + EA_{\mathrm{m}}c\frac{dl}{dt}\frac{1}{t_0} \tag{12}$$

In this model, T denotes the effective tension, combining shear force V with external and internal pressures (p_o and p_i) applied over outer and inner cross-sectional areas (A_o and A_i). A_{m} is the metallic cross-sectional area. Shear force V is influenced by material stiffness E, axial strain ε, and pressure effects adjusted by Poisson's ratio β. Additional terms include torque coupling κ_{tt}, twist angle θ, segment length l_s, damping coefficient c, and the rate of length change $\frac{dl}{dt}$, providing a comprehensive view of the mooring line's response to combined forces. Fig. 2 illustrates the connection scheme of the integrated damping mooring system.

As shown in Fig. 3, after the integrated damping system is coupled with the original mooring lines, the equivalent stiffness and damping of the mooring section increase substantially. Given a pre-tension of l for the bound Mooring 01 with the damper and pre-tensions of $\frac{l}{2}$ for Moorings 02 and Mooring 03 derived from angular analysis, the floating foundation displaces by x(t) under the external force. The equivalent total stiffness and total damping can be expressed in terms of the relative velocities between two reference points at each end of the mooring branch.

Let the instantaneous velocities at the two ends of mooring i be $v_{\text{end }1,i}(t)$ and $v_{\text{end }2,i}(t)$, respectively. The relative velocity is then

$$\Delta v_i(t) = v_{\text{end }1,i}(t) - v_{\text{end }2,i}(t) \tag{13}$$

The relative displacement is obtained by integrating the velocity difference over time:

$$\Delta x_i(t) = \int_{t0}^{t} \Delta v_i(\tau) d\tau + \Delta x_{i0} \tag{14}$$

where Δx_{i0} is the initial pretension extension or initial displacement. Then the system equivalent total stiffness is as following.

$$K_{\mathrm{total}}(t) = \begin{cases} K_{\mathrm{eq1}} \cdot [l + \Delta x_1(t)], & \Delta x_1(t) < \dfrac{l}{2} \\ K_{\mathrm{eq1}} \cdot [l + \Delta x_1(t)] + \left(K'_{\mathrm{eq2}} + K'_{\mathrm{eq3}}\right) \cdot \left[\Delta x_{23}(t) - \dfrac{l}{2}\right], & \dfrac{l}{2} \le \Delta x_1(t) < l \end{cases} \tag{15}$$

Here, $\Delta v_{23}(t)$ is the combined velocity difference component of Mooring 02 and Mooring 03 projected along the external load direction. The total damping force is defined directly from the relative velocities:

$$F_{\mathrm{d,\ total}}(t) = C_{\mathrm{eq1}} \cdot \Delta v_1(t) + C'_{\mathrm{eq2}} \cdot \Delta v_2(t) + C'_{\mathrm{eq3}} \cdot \Delta v_3(t) \tag{16}$$

The equivalent total damping coefficient of the system is then:

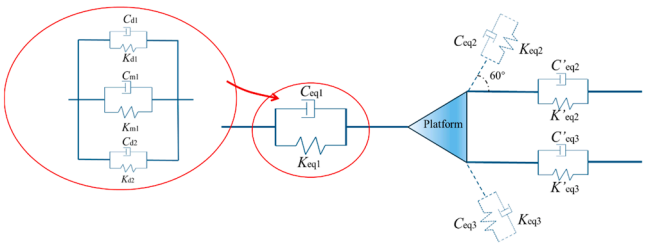

Fig. 3. Equivalent stiffness and damping diagram.

$$C_{\text{total}}(t) = \frac{C_{\text{eq1}}\Delta v_1(t) + C'_{\text{eq2}}\Delta v_2(t) + C'_{\text{eq3}}\Delta v_3(t)}{\Delta v_{\text{system}}(t)} \tag{17}$$

where $\Delta v_{\text{system}}(t)$ is the overall relative velocity between the selected system reference points. The formula K_{total} and C_{total} represent the equivalent total stiffness and equivalent total damping of the system, respectively. Since the direction of the external load forms a 0-degree angle with Mooring 01, K_{eq1} and C_{eq1} represent the equivalent stiffness and damping of Mooring 1. Similarly, K'_{eq2} and K'_{eq3} represent the stiffness components of Mooring 2 and Mooring 3 in the direction of the applied force.

2.3. Dynamic characteristics of Seaflex damper

The mooring element is subjected to the tensile force from the integrated damper, Seaflex (F_S). According to the study [32], the energy dissipation characteristics of the Seaflex damper are expressed as follows:

$$E_d = \int_a^b f(x)dx - \int_a^b g(x)dx \tag{18}$$

$$\int_a^b f(x)dx \approx \frac{b-a}{n}\left[\frac{f(a)+f(b)}{2} + \sum_{k=1}^{n-1} f\left(a + k\frac{b-a}{n}\right)\right] \tag{19}$$

$$F_s = \frac{\int_a^b f(x)dx - \int_a^b g(x)dx}{\Delta x} \tag{20}$$

In the formula, $f(x)dx$ represents the upper part of the load-extension curve, describing the behavior during loading, while $g(x)dx$ represents the lower part of the curve, corresponding to the unloading phase. The parameters a and b are two points on the tension-elongation hysteresis loop, where a represents the coordinates of the minimum elongation and the force threshold, and b represents the coordinates of the maximum elongation and the corresponding force threshold of the damper. E_d denotes the energy dissipation, representing the amount of energy lost during a single load cycle, quantified by the difference in the area under the curves. The variable x indicates any point on the curve, n is the number of subintervals the integration range is divided into for numerical accuracy, and k is the subinterval index used for iterating and summing function values over these subintervals. The tension-elongation curve is provided for this Seaflex damper, as depicted in Fig. 4.

Fig. 5 illustrates the components and materials of this damper. The Seaflex damper system comprises articulated wheels and steel plates on both ends, with rubber hawsers and an overload protection mechanism at the center. The system utilizes titanium alloy components, incorporates 24 rubber hawser-dampers centrally, and maintains a safety factor exceeding 2. When environmental loads exceed design limits, the overload protection automatically engages to ensure tension never surpasses 430 kN, while allowing ultimate material elongation beyond 100 %.

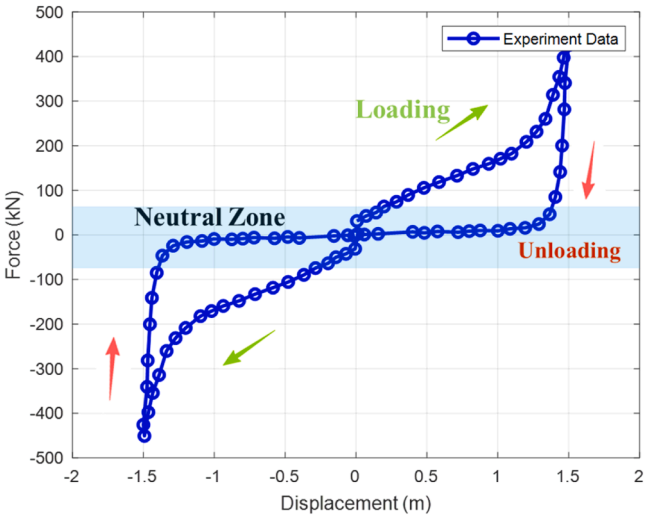

Fig. 4. Tension-displacement relationship curve.

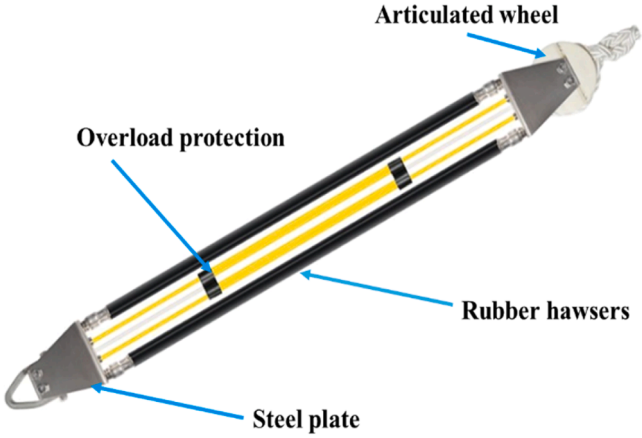

Fig. 5. Structural schematic of the Seaflex damper.

2.4. Mooring damage assessment model

According to DNVGL–OS–E301 (DNV, 2015), limit state checks for mooring design are classified into ULS, Fatigue Limit States (FLS), and ALS. This study focuses on ULS checks to ensure that an individual mooring line has sufficient strength to withstand the load effects imposed by extreme environmental conditions. FLS and ALS checks will be explored in future work. For ULS verification, it is assumed that all mooring lines remain intact, and three tension components are required for the check [34]:

$$TC_{\text{env}} = T_{\text{MPM}} - T_{\text{pret}} \tag{21}$$

$$u = \frac{T_{\text{pret}} \cdot \gamma_{\text{mean}} + TC_{\text{env}} \cdot \gamma_{\text{dyn}}}{s_{\text{C}}} \tag{22}$$

where TC_{env} represents the characteristic environmental tension, T_{MPM} is the most probable maximum line tension, and T_{pret} is the line pretension. The term s_{C} denotes the characteristic mooring strength, taken as 95 % of the minimum breaking strength (MBS). Different standards specify varying safety factors for pretension (γ_{pret}) and environmental tension (γ_{env}), which impact the overall safety margin and design conservatism of the mooring system. Higher safety factors contribute to a more conservative design, ensuring the mooring system can withstand extreme loads with additional reserve strength. For example, the DNV standard, with $\gamma_{\text{pret}} = 1.3$ and $\gamma_{\text{env}} = 1.75$, provides a balance between operational efficiency and safety, suitable for a wide range of offshore conditions. This

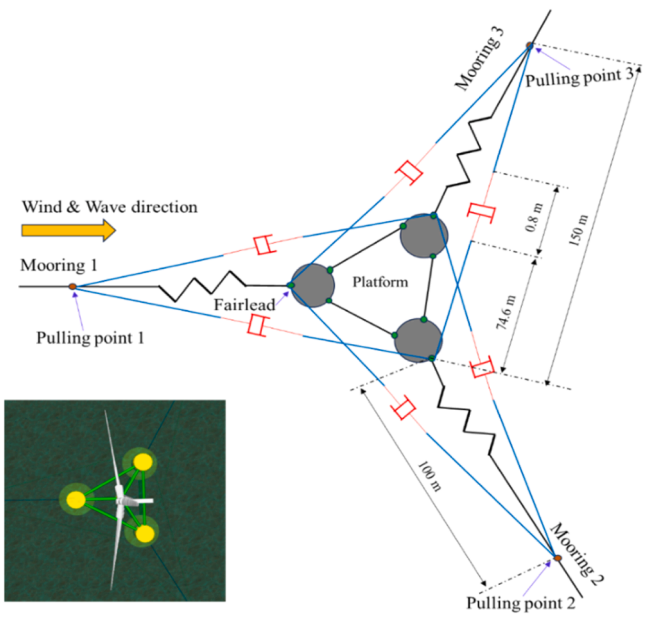

Fig. 6. Installation diagram of the integrated damping mooring system.

reflects a more cautious stance to address long-term material behavior such as creep and fatigue, ensuring the system's longevity.

The most probable maximum (MPM) line tension calculation in OrcaFlex is based on the selected distribution form, with the Rayleigh distribution applied in this study. This approach allows direct computation of the MPM value through spectral moments. Ochi [35] explained how spectral moments are derived and their application in fitting Rayleigh distributions. Under the assumption of a Gaussian distribution, Ochi demonstrated that the most probable maximum (T_{MPM}) within a storm duration T_{storm} can be computed as:

$$T_{\mathrm{MPM}} = \mu + \sigma\sqrt{2\ln n} \tag{23}$$

Where μ is the mean of the tension time series, σ is the standard deviation of the tension time series, $n = \frac{T_{\mathrm{storm}}}{T_z}$, where T_z represents the mean up-crossing period. To incorporate risk considerations into the extreme value analysis, the MPM can be adjusted with a risk parameter α. This yields:

$$MPM_{\alpha} = \mu + \sigma\sqrt{2\ln\left\{\frac{-n}{(\ln(1-\alpha))}\right\}} \tag{24}$$

where α reflects the probability of exceedance and helps evaluate extreme load cases with a defined confidence level.

3. Research preparation

To validate the advantages of the integrated damping mooring technology under operational sea states for FOWT, previous work compared it with conventional mooring systems [36]. The installation diagram of the damping scheme is shown in Fig. 6. Using the 5-year sea state data from the MET wind turbine test center in Norway, statistical analyses of wind speed, wave height, and period distributions were conducted based on ERA5 data. As shown in Fig. 7, the probability density diagram of the occurrence of major sea conditions is drawn according to the actual wind speed and wave height data in this region.

To investigate the impact of the damping system on the NREL 5MW semi-submersible wind turbine, this study utilised the Orcaflex dynamic simulation software from the OC4 project in collaboration with NREL. As a participant in the hydrodynamic portion of the NREL OC4 project, the OrcaFlex model data aligns perfectly with the data published by NREL [37]. Numerical models of different mooring systems, including the traditional and integrated damping systems, were constructed using the Orcaflex software to analyze the fatigue damage distribution under integrated damping technology.

The numerical simulation results indicate that the fatigue life of mooring lines is significantly improved by implementing the integrated damping system. Specifically, the Seaflex damper, representing rigid damping units, demonstrates remarkable advantages across 45 operational sea states (see Fig. 8). Comparative analysis shows that the maximum reduction in fatigue damage achieved with the Seaflex damper reaches 43 %, with the mooring line lifetime extended to 31.6 years at the connection point between the anchor chain and the damping unit and to 31.9 years at the seabed anchor point (see Fig. 9). Owing to its unique response characteristics, the Seaflex damper provides a flexible response under normal operating sea states, effectively absorbing energy from wind and wave loads and reducing tension force in the mooring lines.

This study will build on existing research results to conduct an in-depth investigation into the impact of this technology on the FOWT system under extreme sea states. Different materials for connecting lines, such as nylon rope, polyester fiber rope, wire rope, and steel chains, will be tested on both sides of the flexible damper. The focus is on analyzing the effects of different material combinations on the Ultimate Limit State (ULS) and the Accidental Limit State (ALS) of the FOWT system under extreme conditions.

3.1. Mooring configuration

In this section of the study, several deployment methods of this flexible damper are discussed in detail. Examples include connecting it in series with the original mooring line and attaching it to the fairlead, or installing it in parallel between mooring lines, as

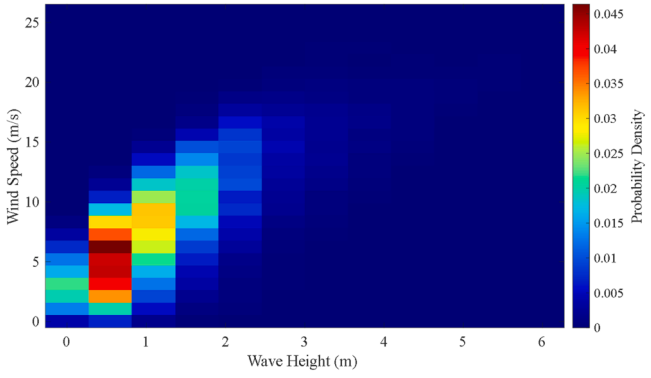

Fig. 7. Selection of operational sea states.

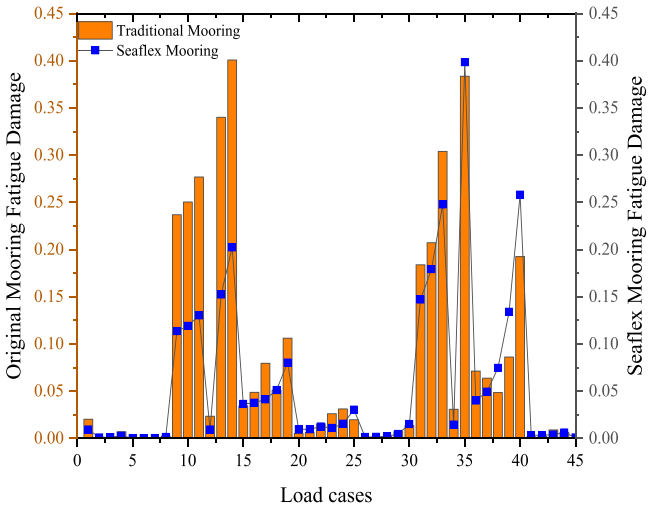

Fig. 8. Fatigue damage reduction and lifetime improvement with the Seaflex damper.

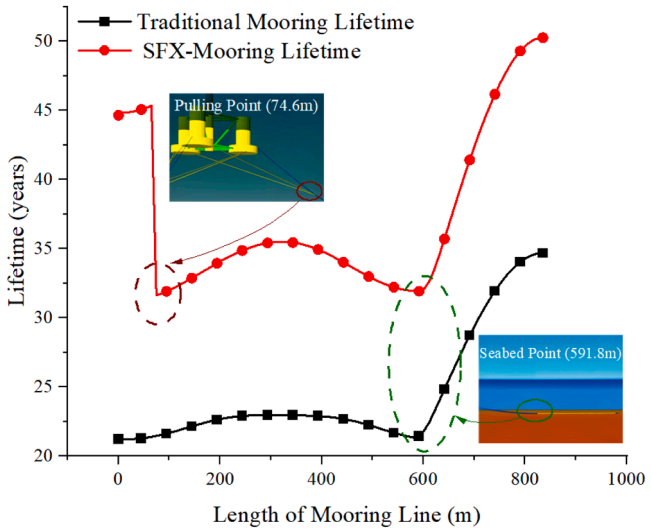

Fig. 9. Fatigue damage distribution analysis for traditional and integrated damping mooring systems.

illustrated in Fig. 10. Taking the operational sea states of the MET wind turbine test center as a reference, the performance of the three connection schemes is compared under Sea State 35 (Wave period Tp = 13.5 s, significant wave height Hs = 1.5 m, wind speed Ws= 10.5 m/s), which induce the most severe structural damage. Fatigue damage accumulation in mooring lines under Sea State 35 over 1 year, calculated via the T-N curve method for these three damping schemes, is compared in Fig. 11. As shown, the cross-anchored

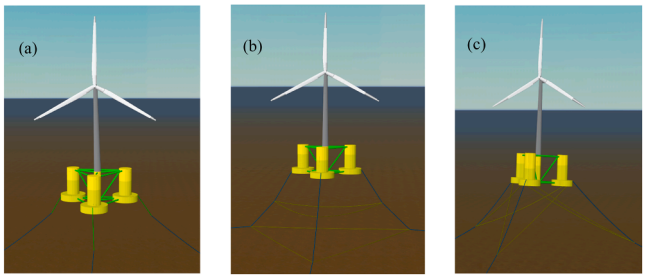

Fig. 10. Mooring configuration schemes: (a) series damping scheme. (b) parallel damping scheme. (c) cross-parallel damping scheme.

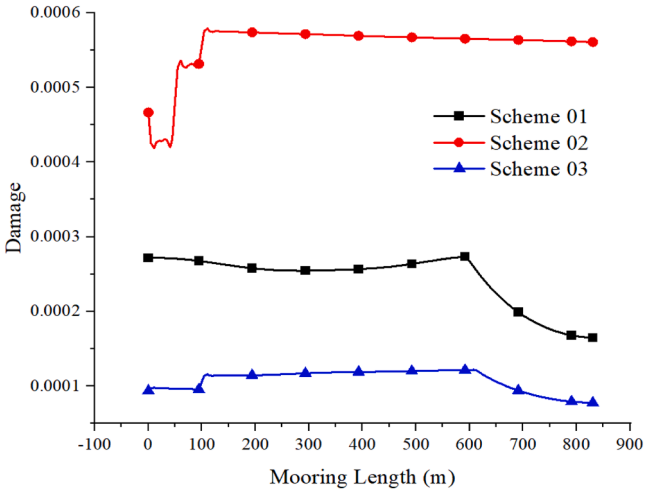

Fig. 11. Mooring configuration schemes: (a) series damping scheme. (b) parallel damping scheme. (c) cross-parallel damping scheme.

damping configuration significantly reduces fatigue damage in the mooring system compared to the other two schemes.

4. Case research

This study analyzes mooring line failure issues using the NREL 5 MW wind turbine mounted on the OC4 DeepCwind semi-submersible platform. The structural configuration of the FOWT system is shown in Fig. 2. Detailed specifications of the 5 MW reference turbine and the OC4 DeepCwind semi-submersible platform are presented in Table 1 [12]. The platform is designed with a central column supporting the turbine tower, which is connected to three outer columns via supporting structures. A wider cylindrical structure is incorporated at the base of the outer column to reduce platform motion. The platform's specific dimensions are shown in Fig. 6, and the breaking strength of the mooring lines is 11,304 kN.

A Seaflex damper with a maximum damping force of 3000 kN was chosen during the selection and design process. Given that a 50-year return period sea condition may lead to the risk of anchor chain failure and an increase in the elongation of the connecting lines, the minimum breaking load (MBL) of the connecting lines was set to ensure a safety factor of 1.5 (4500 kN). Moreover, the selection of mooring connectors at both termination ends of the Seaflex damper requires careful consideration, as different material compositions may lead to distinct operational implications. Based on this, parameter calculations and material selection were performed for different types of ropes according to marine engineering design principles, ensuring that their strength, stiffness (EA), and mass (Mass) met the design requirements (Table 2). The operational and survival conditions of the floating offshore wind turbine (FOWT) are defined in the DNVGL-RP0286 standard. This study primarily considers the 1-year return sea states and 50-year return sea conditions reported by NREL [38] (see Fig. 12). The JONSWAP spectrum and NPD wind spectrum were used to simulate the operational environment for the FOWT.

The comparison of spectral density between the 1-year and 50-year return period sea states, as shown in the Fig. 12, reveals significant differences in the distribution of wave and wind energy, which have critical implications for the dynamic responses of FOWT. At 0.015 Hz (the surge characteristic frequency) [39], the spectral density of sea elevation in the 50-year return period is significantly higher than that in the 1-year return period, indicating that the enhanced wave energy in this frequency range will substantially amplify the surge motion of FOWT. At 0.039 Hz (the heave characteristic frequency), the wave energy in the 50-year

Table 1
The Properties of the 5 mw reference turbine and OC4-DeepCwind platform.

Property	Value
Rating	5 MW
Rotor, Hub diameter	126.0 m,3.0 m
Hub height	90.0 m
Cut-in, Rated, Cut-out wind speed	3.0 m/s,11.4 m/s,25 m/s
Cut-in, Rated rotor speed	6.9 rpm,12.1 rpm
Overhang, Shaft tilt, Pre-cone	5.0 m, 5.0° , 2.5°
Rotor mass	110,000 kg
Nacelle mass	240,000 kg
Total mass	347,460 kg
Roll inertia about the center of mass	6.827E9 kg · m^2
Pitch inertia about the center of mass	6.827E9 kg · m^2
Yaw inertia about the center of mass	1.226E10 kg · m^2

Table 2
Material selection parameters for damper connection lines.

Item	Diameter (m)	Mass (te /m)	EA (kN)	MBL (kN)
Chain	0.0722	0.0225	4.2E+5	4.5E+3
Wire	0.0604	0.0225	6.02E+5	4.5E+3
PE	0.473	0.206	1.5E+5	4.5E+3
Nylon	0.2764	0.068	1.62E+5	4.5E+3

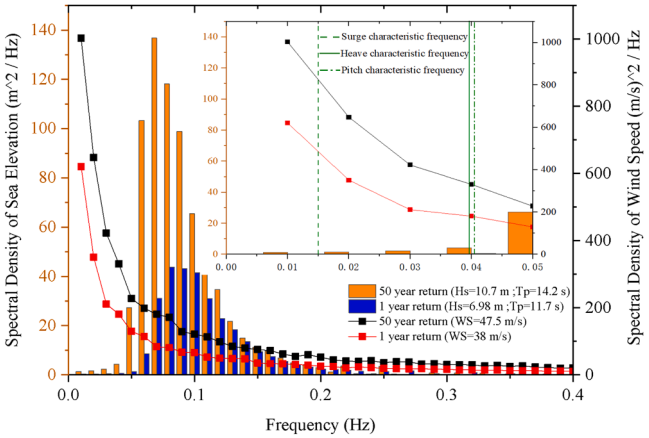

Fig. 12. 1-year and 50-year return sea states.

return period is also notably higher, which is expected to result in greater heave response amplitudes. Furthermore, at 0.042 Hz (the pitch characteristic frequency), although the difference in wave spectral density is minor, the wind spectral density in the 50-year return period is significantly elevated, suggesting that wind disturbances could amplify the pitch motion through aerodynamic coupling effects. Overall, the enhanced wave and wind energy in the 50-year return period will significantly increase the surge and heave responses and may indirectly influence the dynamic characteristics of pitch motion.

In addition, it is noteworthy that the wave spectral density in the 50-year return period is significantly higher over a broader frequency range (0.015–0.042 Hz) compared to the 1-year return period, indicating the potential simultaneous excitation and coupling of multiple motion modes. This complex multimodal response could increase the global dynamic load on the platform, particularly impacting the fatigue performance of the mooring system and tower structure. Therefore, comprehensive frequency-domain and time-domain assessments of the response amplitude operator (RAO) under extreme sea states are crucial for accurately predicting structural performance, optimizing design, and mitigating failure risks under extreme conditions.

4.1. Response under the one-year return period sea state

Based on the mooring system layout proposed in the previous section, this chapter further analyzes the dynamic response performance of different mooring systems under a 1-year return period sea state. The study focuses on key motion parameters of the

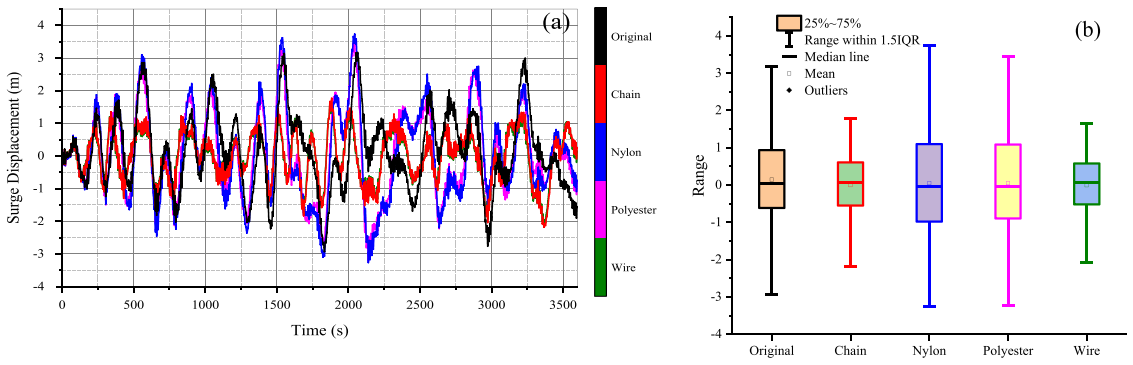

Fig. 13. Time Domain displacement and statistical distribution of surge for different mooring systems: (a) time domain displacement of surge; (b) corresponding box plot of surge displacement.

FOWT, such as surge, heave, and pitch, as well as the tension of the main mooring lines. By comparing time-domain data and statistical distributions (box plots), the performance differences of each mooring configuration under extreme sea conditions are revealed (see Fig. 13–16). The analysis results demonstrate the advantages and disadvantages of different mooring systems in mitigating motion responses, reducing tension peaks, and maintaining platform stability. This provides important evidence for validating the layout scheme's effectiveness and optimizing the design. The following sections will discuss the specific performance of each mooring system under a 1-year return period sea state in detail.

During the 1-year return period sea state, significant differences in the surge and heave motion responses of the FOWT were observed for different mooring systems. From the time-domain data of the surge (see Fig. 13(a)), the original system exhibited the largest lateral displacement response of 3.17 m, indicating a high sensitivity to extreme sea conditions under an unoptimized design. In contrast, the wire mooring system showed a significant reduction in maximum response, dropping to 1.65 m, which represents a 48.02 % decrease compared to the original system and demonstrates the best suppression capability. The chain mooring system had a maximum displacement of 1.77 m, a 44.15 % reduction from the original system, performing slightly worse than the wire mooring system. The polyester mooring system, however, showed a maximum lateral displacement of 3.73 m, which was higher than that of the original system, indicating poor dynamic stability. Similarly, the nylon mooring system had a maximum lateral displacement of 3.45 m, also higher than the original system, reflecting significant dynamic instability. Box plots (see Fig. 13(b)) further reveal the differences in dynamic response among the different mooring systems.

The median lateral displacement of the wire mooring system was closest to zero, with the smallest fluctuation range and no significant outliers, demonstrating the best dynamic stability and suppression ability. The chain mooring system had a median slightly higher than the wire mooring system, but its fluctuation range was smaller, also showing good stability. On the other hand, the polyester and nylon mooring systems exhibited medians that deviated further from zero, with significantly wider fluctuation ranges and more outliers, indicating inadequate dynamic performance and susceptibility to wave loading. The original system performed the worst in all statistical metrics, with the largest median, fluctuation range, and the most outliers.

For the heave motion, significant differences among the mooring systems were also observed (see Fig. 14). The original system exhibited a maximum heave response of 2.90 m, significantly lower than all other systems. The maximum heave responses for the chain, nylon, polyester, and wire mooring systems were 4.89 m, 4.53 m, 4.47 m, and 5.06 m, respectively, representing increases of 68.78 %, 56.11 %, 54.37 %, and 74.50 % compared to the original system. Despite the substantial effect of different mooring materials on the heave motion response, the amplitudes remained within reasonable design limits. From a statistical perspective, the wire mooring system exhibited the largest response amplitude and contained significant outliers, suggesting possible large dynamic fluctuations under the 1-year return period sea state. This may be attributed to its high elastic modulus, resulting in weaker heave damping performance.

The chain mooring system showed a more stable dynamic response, with a fluctuation range smaller than that of the wire mooring system and no significant outliers, making it a stable and reliable option. The fluctuation ranges of the nylon and polyester mooring systems were significantly wider, especially the polyester system, which showed a marked increase in the number of outliers, further confirming its unstable dynamic performance. Overall, although the heave motion amplitudes of the mooring systems increased compared to the original system, they all remained within reasonable dynamic response ranges, indicating their design is suitable for the 1-year return period sea state.

Under the 1-year return period sea state, significant differences in the control of pitch motion of the FOWT were observed for different mooring systems (see Fig. 15(a)). From the time-domain results, the original system exhibited the maximum pitch angle of 3.2°, the largest among all systems, indicating its high sensitivity to pitch dynamic disturbances under unoptimized design conditions. In contrast, the wire mooring system showed the lowest maximum pitch angle of 1.7°, a reduction of 46.87 % compared to the original system, demonstrating the best dynamic suppression capability. The chain mooring system had a maximum pitch angle of 1.9°, reduced by 40.63 %, performing second best to the wire mooring system. The maximum pitch angles of the polyester and nylon mooring systems were 3.5° and 3.4°, respectively, both higher than the original system, indicating poor dynamic stability. This

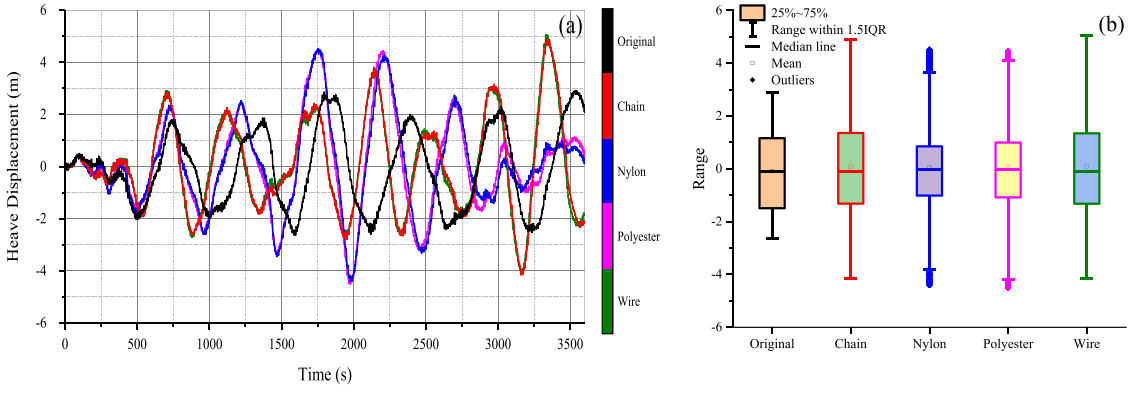

Fig. 14. Time domain displacement and statistical distribution of heave for different mooring systems: (a) time domain displacement of heave; (b) corresponding box plot of heave displacement.

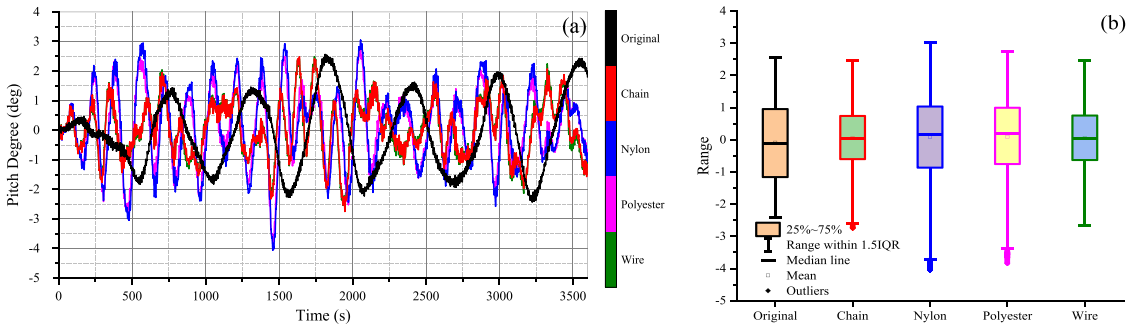

Fig. 15. Time domain angle and statistical distribution of pitch for different mooring systems: (a) time domain angle of pitch; (b) corresponding box plot of pitch angle.

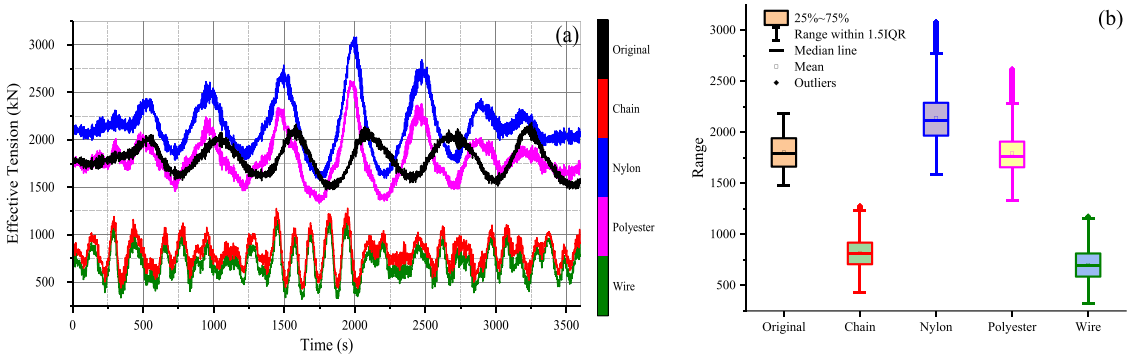

Fig. 16. Time domain and statistical distribution of effective tension for different mooring systems: (a) time domain variation of effective tension; (b) corresponding box plot of effective tension variation.

suggests that the wire and chain mooring systems significantly suppress pitch disturbances, while the polyester and nylon mooring systems still exhibit inadequate dynamic response under extreme sea conditions.

Further analysis using box plots (see Fig. 15(b)) reveals the differences in the stability of pitch responses among the mooring systems. The median pitch response of the wire mooring system was closest to zero, with the smallest fluctuation range and no significant outliers, confirming its superior dynamic stability. The chain mooring system had a slightly larger fluctuation range compared to the wire mooring system but with no significant outliers, exhibiting good reliability. In contrast, the median pitch responses of the polyester and nylon mooring systems deviated significantly from zero, with much wider fluctuation ranges and multiple outliers, indicating unstable dynamic performance. Additionally, the original system exhibited the largest fluctuation range and the highest number of outliers, further illustrating its poor adaptability in pitch response.

Regarding the tension response of the main mooring lines (see Fig. 16), notable differences in performance were observed among the mooring systems. From the time-domain data, the maximum effective tension of the original system was 2500 kN, the highest among all systems, indicating a high sensitivity to load variations under extreme sea conditions. In contrast, the maximum tension of the wire mooring system was 700 kN, a 72 % reduction compared to the original system, demonstrating the best load dissipation capacity. The chain mooring system had a maximum tension of 900 kN, a 64 % reduction, performing second best to the wire mooring system. The maximum tensions of the nylon and polyester mooring systems were 2100 kN and 2000 kN, respectively, representing only a 16 % and 20 % reduction compared to the original system. The box plot analysis further shows (see Fig. 16(b)) that the median tension of the wire mooring system was the lowest, with the narrowest fluctuation range and no outliers, reflecting the best dynamic stability. The chain mooring system followed closely, with a slightly higher median and fluctuation range but still demonstrating good dynamic performance. In contrast, the nylon and polyester mooring systems had higher median tensions, wider fluctuation ranges, and more outliers, indicating weaker dynamic stability. The original system exhibited the highest fluctuation range and the most outliers, further emphasizing its performance disadvantages under extreme sea conditions. These results suggest that the wire and chain mooring systems excel in tension control and dynamic stability, making them the preferred choice for extreme sea conditions. While the tension response of the nylon and polyester mooring systems showed some improvement, their high fluctuation ranges and the number of outliers indicate that their stability under complex conditions still requires optimization.

4.2. Response under the fifty-year return period sea state

Building upon the findings under one-year return period sea conditions, this section delves into the comparative performance of the

selected mooring systems (wire and chain) under the more extreme 50-year return period sea state.

From the surge response plot (see Fig. 17), it can be observed that in the 0.001–0.01 Hz frequency range, the original mooring system exhibits the highest amplitude, which may be attributed to its insufficient restoring stiffness in the surge direction. In contrast, the chain and wire mooring systems increase the stiffness compared to the original system, significantly limiting low-frequency surge drift. In the 0.05–0.1 Hz range (the wave loading frequency domain), the three curves gradually converge in the frequency domain, indicating that under dominant wave excitation, the differences between the mooring systems are reduced. When the frequency exceeds 0.1 Hz, the constraint force and energy dissipation capacity provided by the original system is inferior to those of the chain and wire mooring systems (with larger fluctuations in peak values), while the chain and wire mooring systems exhibit more stable behavior. The maximum surge peak values from the time-domain data indicate that the peak for the original system reaches 4.6881 m, while the chain and wire mooring systems are 2.67675 m and 1.94098 m, respectively, which represent reductions of approximately 42.9 % and 58.6 % compared to the original system.

From the heave response plot (see Fig. 18), when the frequency is less than 0.01 Hz, the amplitude of the original system is relatively low, while the chain and wire systems exhibit higher displacements. In the 0.01–0.05 Hz range, the three curves gradually converge, indicating that wave excitation becomes the dominant force, and the differences between the mooring systems are reduced. When the frequency exceeds 0.1 Hz, the wire mooring system shows slightly higher response peaks at some frequencies, while the chain and original systems remain more stable, demonstrating that different mooring designs still exhibit distinct characteristics under the hydrodynamic coupling effects in this frequency range. This phenomenon is also validated by the time-domain data: the maximum heave peak for the original system is approximately 3.1779 m, while for the chain and wire mooring systems, the peaks are 5.04713 m and 5.08012 m, respectively. Although the latter two configurations show an increase in displacement in the heave degree of freedom compared to the original system, the increase remains within the design safety limits and does not adversely affect the overall stability and safe operation of the wind turbine.

From the pitch response plot (see Fig. 19), it can be observed that at frequencies below 0.01 Hz, the original mooring system exhibits the highest pitch amplitude, indicating its weaker capability in pitch control. In contrast, the chain and wire mooring systems, by providing higher pitch stiffness and damping, effectively reduce the platform's risk of capsizing under low-frequency conditions. In the 0.05–0.1 Hz range, the differences in pitch response among the three mooring systems gradually decrease, suggesting that in this frequency band, the heave motion is mainly dominated by wave excitation, and the influence of mooring system differences becomes less significant. However, when the frequency exceeds 0.1 Hz, the wire mooring system shows higher response peaks at certain frequencies, while the chain and original systems remain relatively stable, indicating that the stiffness characteristics of different mooring systems still have a significant effect on the platform's pitch in this frequency range.

Overall, the chain and wire mooring systems significantly reduce the platform's risk of capsizing, and their effect on suppressing the maximum pitch angle is evident in the time-domain data. The specific time-domain results indicate that the maximum pitch angle for the original system is 4.97927°, while the chain and wire mooring systems are reduced to 3.79952° and 4.03997°, respectively. The calculated results show that the maximum pitch angle of the chain system is reduced by about 23.7 % compared to the original system, while the wire mooring system reduces it by approximately 18.9 %, demonstrating the significant role of the new mooring design, especially the chain system, in mitigating large pitch angles and capsize risks.

From the effective tension plot (see Fig. 20), it can be seen that with the help of the chain and wire mooring systems, the effective mooring tension at the cable entry points of the FOWT is significantly reduced. Time-domain data indicate that the maximum effective tension for the original system is 4213.14 kN. For the chain system, the maximum effective tension is 3234.13 kN, while the wire

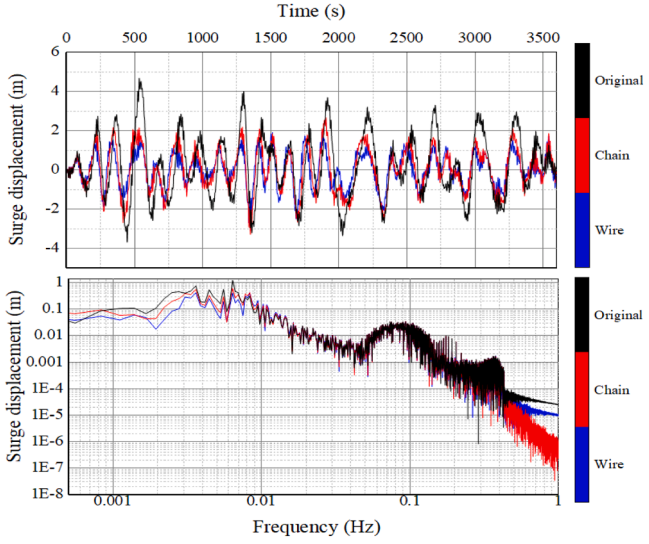

Fig. 17. Surge time domain and frequency-domain response under 50-year return sea states.

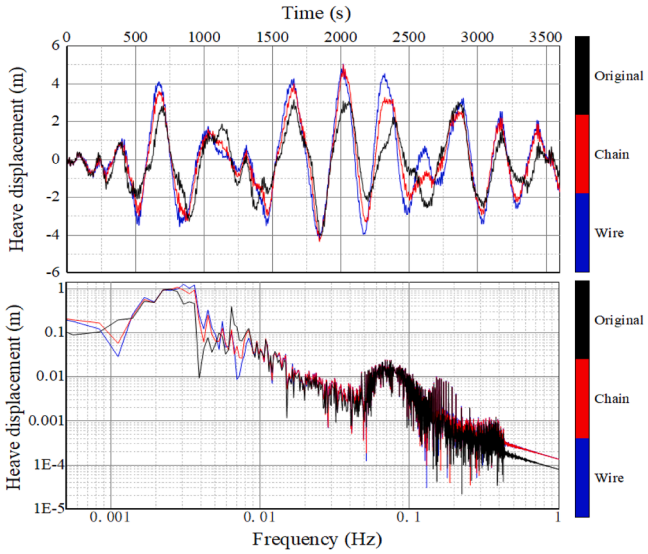

Fig. 18. Heave time domain and frequency-domain response under 50-year return sea states.

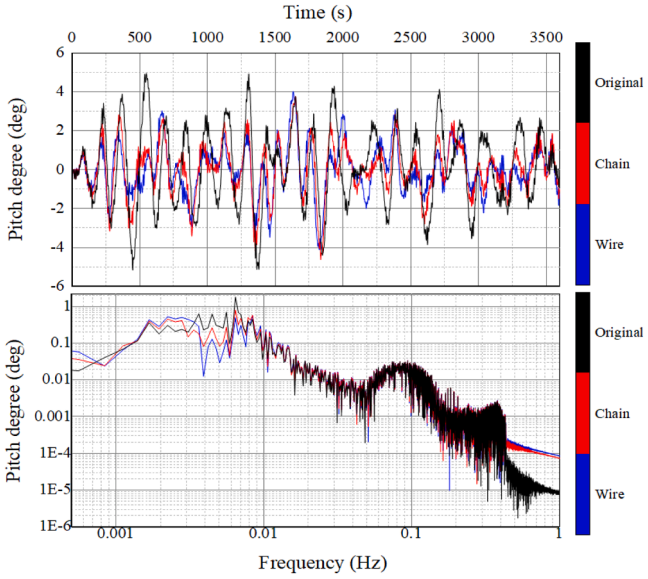

Fig. 19. Pitch time domain and frequency-domain response under 50-year return sea states.

mooring system only reaches 2043.68 kN. The calculated results show that the maximum effective tension of the chain system is reduced by about 23.2 % compared to the original system, and the wire mooring system reduces it by approximately 51.5 %, highlighting the advantages of the new mooring design in suppressing cable tension. Frequency domain analysis also reveals that although the differences in tension characteristics among the three mooring systems are small in the 0.05–0.1 Hz range, the differences in stiffness and pretension on both sides of this frequency band are more pronounced, leading to better suppression of effective mooring tension in extreme situations such as large drifts or local resonances for the chain and ire systems.

Overall, the effective mooring tension is closely related to the surge and pitch motion amplitudes of the platform. In the frequency range below 0.01 Hz, mooring systems with low damping or weak stiffness (such as the original system) are more prone to excite surge motion, thus increasing the peak tension in the mooring lines. While the chain and wire mooring systems also show a trend of increasing tension in this range, the increase in tension is less pronounced due to the friction, bending energy dissipation, and higher stiffness constraints of the chain system. In the 0.05–0.1 Hz range, the differences in surge and pitch responses among the three mooring systems are small, and the corresponding effective tension curves tend to converge. After the 0.1 Hz frequency range, the wire mooring system, with its higher stiffness but relatively less self-damping, may exhibit higher tension peaks at certain frequencies. On the other hand, the chain system, through friction and bending energy dissipation, demonstrates a stronger ability to attenuate high-

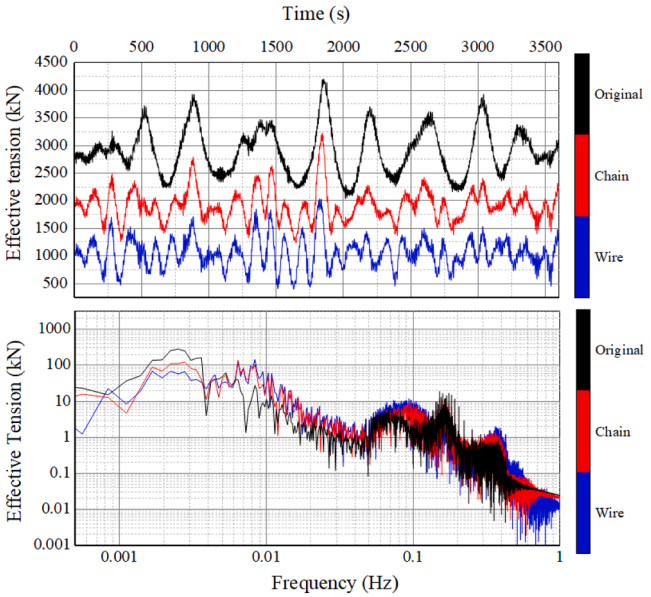

Fig. 20. Effective tension time domain and frequency-domain response under 50-year return sea states.

frequency vibrations, which is consistent with its performance in surge and pitch responses. Meanwhile, the original system also lacks sufficient damping and restoring capacity in this frequency range, leading to insufficient tension decay and the occurrence of short-term peaks. In conclusion, the chain and wire mooring systems not only significantly reduce the maximum mooring tension at the cable entry points, but also exhibit excellent vibration suppression capabilities, contributing to the overall safety and reliability of the floating wind turbine.

4.3. Response under the accidental limit state

To further validate the safety-enhancing effects of the integrated damping system under extreme sea conditions, this section simulates the dynamic behavior of the FOWT under single-point mooring line breakage conditions for the two well-performing mooring configurations, chain and wire. The study aims to assess the drift and tension suppression capabilities of different mooring systems in the event of failure in mooring 1, 2, or 3 and the system stability performance under 1-year and 50-year return period sea states (see Fig. 21, 22, 23). The analysis results show that extreme sea conditions significantly exacerbate the drift distance and tension peak values of the FOWT. In contrast, the optimized chain and wire mooring systems demonstrate good drift control and tension suppression capabilities, providing technical support for enhancing the operational safety of the FOWT under accidental limit states

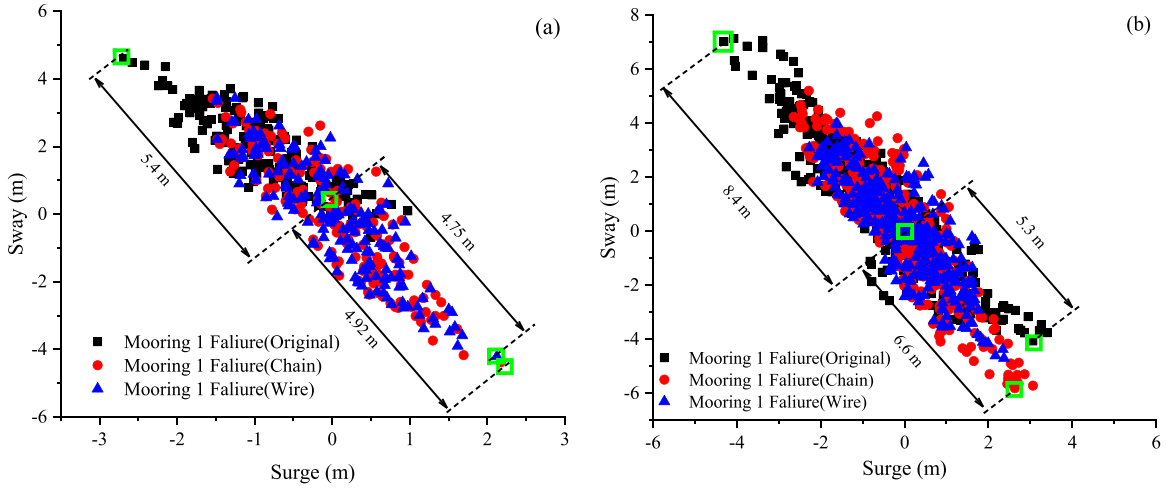

Fig. 21. Mooring line failure comparison under 1-year and 50-year return sea conditions: (a) mooring 01 failure comparison (1-year return); (b) mooring 01 failure comparison (50-year return).

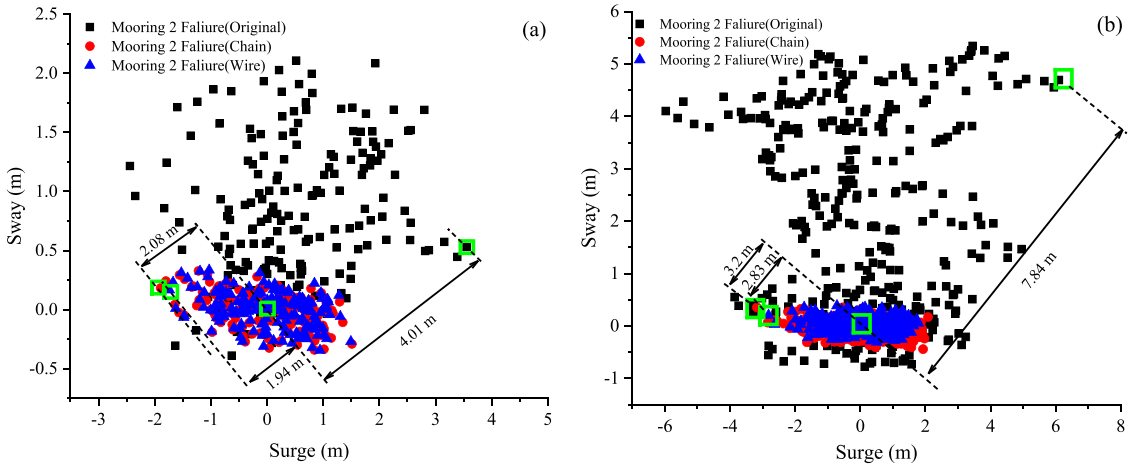

Fig. 22. Mooring line failure comparison under 1-year and 50-year return sea conditions: (a) mooring 02 failure comparison (1 year); (b) mooring 02 failure comparison (50 year).

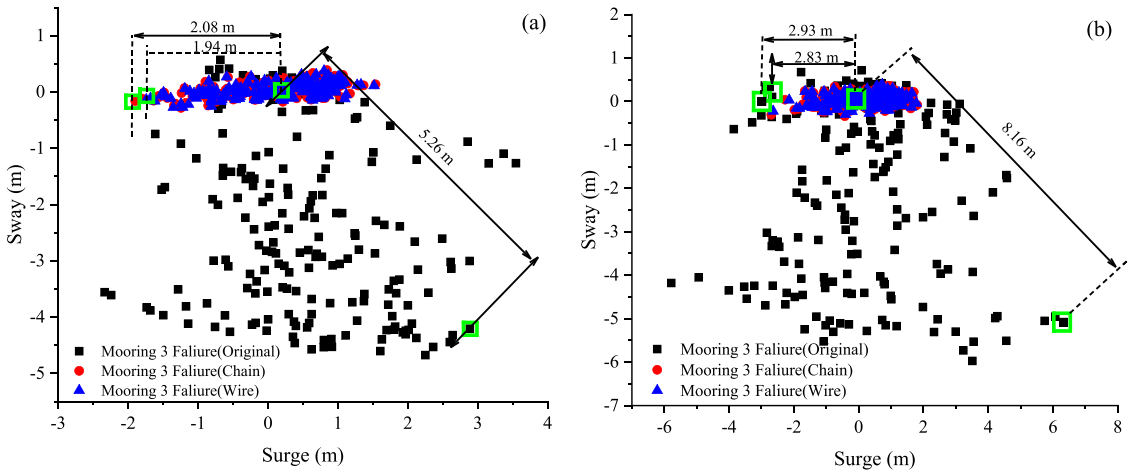

Fig. 23. Mooring Line failure comparison under 1-year and 50-year return sea conditions: (a) mooring 03 failure comparison (1 year); (b) mooring 03 failure comparison (50 year).

(ALS). The specific results are analyzed in detail below.

Under both 1-year and 50-year return period sea conditions, the maximum drift distance of the FOWT due to mooring line failure shows a significant increasing trend with the worsening of sea conditions. The drift behavior of the original mooring system is particularly pronounced under different anchor line failure scenarios (see Table 3). In the case of mooring 1 Failure (Fig. 21), the maximum drift increases from 5.4 m to 8.4 m, representing a 55.6 % increase. In the case of mooring 2 failure (Fig. 22), the maximum

Table 3
Comparison of drift under mooring failure scenarios.

System Condition	1 year			50 year		
	Surge	Sway	Max Distance	Surge	Sway	Max Distance
Mooring 3 Failure (Original)	3.09	−4.26	5.26	6.47	−4.96	8.16
Mooring 3 Failure (Chain)	−2.07	−0.19	2.08	−2.93	0.0067	2.93
Mooring 3 Failure (Wire)	−1.93	−0.21	1.94	−2.83	0.085	2.83
Mooring 2 Failure (Original)	3.98	0.46	4.01	6.37	4.58	7.84
Mooring 2 Failure (Chain)	−2.07	0.18	2.08	−3.19	0.34	3.2
Mooring 2 Failure (Wire)	−1.93	0.15	1.94	−2.83	0.2	2.83
Mooring 1 Failure (Original)	−2.7	4.65	5.4	−4.2	7.29	8.4
Mooring 1 Failure (Chain)	2.22	−4.39	4.92	2.79	−5.99	6.6
Mooring 1 Failure (Wire)	2.17	−4.2	4.75	2.37	−4.75	5.3

drift distance increases from 4.01 m to 7.84 m, with a rise of 95.5 %. In the case of mooring 3 failure (Fig. 23), the maximum drift distance increases from 5.26 m under the 1-year return period sea state to 8.16 m under the 50-year return period sea state, representing an increase of approximately 55.6 %. These increases indicate that extreme sea conditions significantly elevate the drift distance of the FOWT, with the most pronounced increase occurring during the failure of mooring 2.

As shown in Table 3, the chain and wire mooring systems exhibit different drift suppression capabilities under various mooring line failure scenarios. Under the 50-year return period sea conditions, the chain mooring system effectively reduces the drift distance compared to the original mooring system. For instance, in the mooring 3 failure (chain) case, the maximum drift is reduced by approximately 60 %, down to 2.93 m, while the wire mooring system performs slightly less effectively, reducing the maximum drift by about 55 %, to 2.83 m. Similarly, in the mooring 2 failure (chain) case, the chain mooring system can reduce the maximum drift by about 60 %, down to 3.2 m, while the wire mooring system achieves a 55 % reduction, bringing the maximum drift to 2.83 m. These data suggest that under extreme sea conditions, the chain mooring system has a significant advantage in controlling horizontal drift (surge). Overall, optimizing the mooring system design is crucial for the stability and drift control of the FOWT. The selection of the mooring system can effectively suppress drift and enhance the turbine's ability to withstand extreme conditions. The chain mooring system demonstrates stronger control over extreme horizontal drift, while the wire mooring system provides a more balanced control capability, suitable for drift suppression across a range of conditions. Therefore, choosing the appropriate mooring system based on specific sea conditions and mooring line failure scenarios can effectively protect the safety of the transmission lines. Under both 1-year and 50-year return period sea conditions, different mooring systems exhibit significant differences in effective tension under mooring line failure scenarios, reflecting the drift control performance of the chain and wire mooring systems (Fig. 24).

Under the 50-year return period sea conditions, the maximum tension of the original mooring system shows a significant increase. For example, in the case of mooring 1 (original), the maximum tension increases from 1352.88 kN under the 1-year return period sea condition to 4288.79 kN, representing an increase of over 217 %. In contrast, the chain and wire mooring systems demonstrate effective tension suppression capabilities under extreme sea conditions. The chain mooring system reduces the maximum tension of mooring 1 to 2161.7 kN, with a reduction of approximately 82.2 %, while the wire mooring system further reduces it to 1978.69 kN, a decrease of about 79.5 %.

For mooring 2 and mooring 3, the chain and wire mooring systems show more pronounced tension control effects in the sway direction, overall exhibiting a more balanced tension reduction capacity. These results indicate that optimizing the configuration of chain and wire mooring systems can effectively alleviate anchor chain tension under extreme sea conditions, improving the drift resistance and damage resilience of floating offshore wind turbines.

4.4. Damage comparison

In the design and operation of FOWT, the safety and reliability of the mooring system are critical, particularly when assessing the risk of failure under extreme sea conditions. This section uses the DNVGL–OS–E301 [40] standard to calculate the ULS and ALS safety factors (u-values) for different mooring systems under 1-year and 50-year return period sea conditions. By comparing and analyzing the failure risk and safety margin of mooring systems based on actual parameters and mechanical models, this study provides essential insights for optimizing the design of FOWT mooring systems. The following discussion will focus on the variations in u-values and safety across different mooring system types (original, chain, and wire) under different sea conditions, as shown in the data table.

The u-values for different mooring systems (original, chain, and wire) under 1-year and 50-year return period sea conditions are shown in Table 4. Overall, the u-values for all mooring systems are below the safety threshold of 1, indicating that their designs provide a sufficient safety margin. However, as the sea conditions transition from the 1-year to the 50-year return period, the u-values generally increase significantly. For instance, the u-value of the original system increases from 0.278 under 1-year conditions to 0.570 under 50-year conditions, showing an increase of approximately 105 %, indicating a higher failure risk under extreme conditions. In the chain

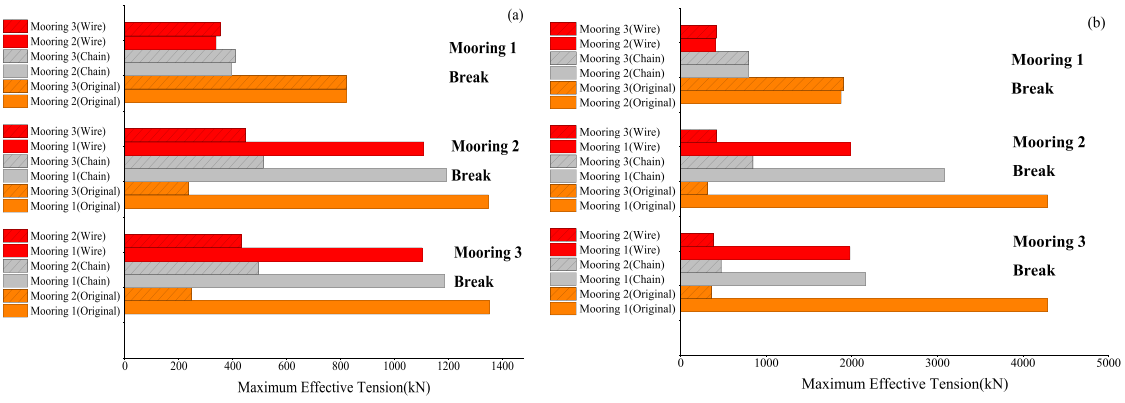

Fig. 24. Mooring line failure comparison under 1-year and 50-year return sea states: (a) tension comparison under 1-year return sea states; (b) tension comparison under 50-year return sea states.

Table 4
Comparison of the U-values of different mooring systems.

Type	Sea State	T_{pret}(kN)	T_{MPM}(kN)	TC_{env} (kN)	u
Original	1 year	1780	2163	383	0.278
Original	50 year	2781	4213	1432	0.570
Chain	1 year	827	1280	453	0.174
Chain	50 year	1934	3238	1304	0.447
Wire	1 year	706	1178	472	0.162
Wire	50 year	1052	2042	990	0.289

Table 5
U-value performance of mooring points (mooring1, mooring2, mooring3).

Mooring	Breaking Mooring	Original		Chain		Wire	
		$u_{1\ year}$	u_{50year}	u_{1year}	u_{50year}	u_{1year}	u_{50year}
Mooring1	2	0.134	0.482	0.131	0.340	0.124	0.227
	3	0.134	0.483	0.130	0.245	0.124	0.227
Mooring2	1	0.080	0.195	0.040	0.084	0.047	0.047
	3	0.024	0.035	0.053	0.052	0.046	0.042
Mooring3	1	0.080	0.199	0.041	0.084	0.036	0.047
	2	0.022	0.031	0.054	0.086	0.048	0.046

and wire mooring systems, the u-values increase from 0.174 to 0.162 under 1-year conditions to 0.447 and 0.289 under 50-year conditions, respectively. Notably, the u-values of the chain and wire mooring systems are significantly lower than those of the original system, and their increases are also smaller (157 % and 78 %, respectively), reflecting superior tensile strength and dynamic stability.

The u-value performance of each mooring point (mooring1, mooring2, mooring3) under the two sea conditions is shown in Table 5. In the original system, the u-value at mooring1 is 0.134 under 1-year conditions, which surges to 0.483 under 50-year conditions, an increase of 260 %, making it the point with the highest failure risk. In contrast, the u-values for the chain and wire mooring systems at the same mooring point increase from 0.130 to 0.245 (88 % increase) and from 0.124 to 0.227 (83 % increase), respectively, indicating that these two systems exhibit stronger stability under extreme conditions. Additionally, some mooring points (such as mooring2) show a slight decrease in u-values under the chain and wire mooring systems. For example, in the chain system, the u-value at mooring2 under 50-year conditions is 0.052, slightly lower than 0.053 under 1-year conditions, which may be attributed to the optimized design of its load distribution.

Based on the analysis of the data from both tables, the chain and wire mooring systems significantly outperform the original system in both ULS and ALS evaluations. By effectively reducing the u-value, they substantially decrease the failure risk under extreme sea conditions. Although the u-value of the original system is relatively high, it remains within the safety range, indicating that its design provides basic reliability. However, material substitution (e.g., steel cables or chains) or enhanced localized force design could be considered at critical mooring points to further optimise its performance. The chain and wire mooring systems' excellent performance in both ULS and ALS evaluations demonstrates their potential for future optimization in FOWT mooring system designs. Additionally, future research could integrate dynamic response simulations and fatigue analysis to further validate the safety and cost-effectiveness of these mooring systems over the long-term operation, thus providing reliable technical support for the large-scale application of FOWT.

5. Comparison of mainstream technologies

The technology proposed in this paper focuses on improving mooring performance without altering the floating foundation structure or adding extra mass, making it a lightweight and adaptable solution. To demonstrate its effectiveness, we compare it with several studies that have explored advancements in mooring damping strategies, alternative mooring configurations, and innovative chain designs. These studies serve as benchmarks, providing insights into various approaches and their impact on key performance indicators such as mooring tension and platform motion. The following table provides a detailed comparison, highlighting how the integrated damping mooring system presented in this paper aligns with or surpasses existing methods in addressing the challenges of FOWT mooring systems.

A summary of current research on FOWT mooring systems is presented in Table 6, highlighting various technological approaches and showcasing the characteristics and effectiveness of different solutions. For instance, [18] explored methods to enhance damping performance by introducing heavy chains or ballast blocks, significantly reducing tension (by 28.68 %) and Surge motion (by 14.58 %), making it suitable for controlling platform motion amplitude. In contrast, [41] designed two multi-segment arrangement mooring systems (tension reduced to 34 %−65 % of the prototype), with surge motion reduced by 44 %, showing the potential of material mixing in balancing tension and motion control. Further optimization of the hybrid design, such as [42], which combined chains and polymer ropes, reduced tension by approximately 27 %, but at the cost of a 30 % increase in pitch and heave motion, indicating shortcomings in dynamic stability. In terms of structural optimization, [43] used polymer springs to absorb energy, significantly

Table 6
Comparison of mainstream mooring technologies.

Paper	Mooring Damping Technology	Research Object	Mooring Tension (kN)	RAO
[18]	Designed two mooring models to investigate the impact of clump weights or heavy chains	Based on 10-MW OO-Star semi-submersible platform.	The maximum tension of mooring decreased by 28.68 %.	The maximum surge values decreased by 14.58 %.
[41]	Designed a multi-segment arrangement mooring system (buoy, clump weight, catenary, and taut mooring lines.)	Based on 5 MW OC4 DeepCwind FOWT	The maximum tension of mooring decreased by 34 %−65 %.	The MSM-BMW surge and pitch are reduced by 44 % and 33 %. The MSM-BSW heave increases by 150 %.
[42]	Studied the impact of mixed mooring schemes (chain + polymer rope + chain).	Based on PivotBuoy FOWT	Reduced mooring tension by approx. 27 %	The pitch and heave motion responses of the floating offshore wind turbine increase by about 30 %
[43]	Designed featuring polymer springs for the mooring system	Based on the Volturnus-S 15-MW FOWT	the spring equipped design reduces peak tensions by up to 60 %	The polymer springs increase mean surge by 53 % and maximum surge by 48 % (7.2 m).
[44]	Designed Multi-point mooring Method	Based on the new semi-submersible floating foundation with three columns	The effective tension of the mooring system increases by more than 12.6 % under ALS.	The transient surge increases by 127.67 % - 319.78 % under ALS.
This Paper	Designed a integrated damping mooring system for FOWT	Based on the NREL 5-MW FOWT	Under ULS conditions, the chain system reduces maximum tension by 23.2 %−64 %, while the Wire system achieves a greater reduction of 51.5 %−72 %.	Under ULS conditions, the chain system reduces FOWT surge displacement by **43 %−44 %** and pitch angle by **24 %−41 %**, while the wire mooring system achieves reductions of **48 %−59 %** in surge displacement and **19 %−47 %** in pitch angle. Under ALS conditions, the chain system reduces drift distance by **60 %**, and the wire mooring system reduces it by **55 %**.

reducing tension peaks (by up to 60 %), but also causing a significant increase in surge motion (with a maximum increase of 48 %−53 %), indicating a need for further optimization in motion control. In comparison, multi-point mooring design improved tension-bearing capacity under ALS conditions (by 12.6 %) but resulted in a dramatic increase in transient surge motion (by 127.67 %−319.78 %) [44], indicating potential risks in platform motion under extreme sea conditions.

In conclusion, these studies offer unique strengths in reducing tension or controlling platform motion, but they often struggle to balance tension control and dynamic stability. In contrast, the integrated damping mooring system proposed in this paper achieves a comprehensive optimization of both mooring line tension and platform motion, without altering the floating foundation structure or adding extra mass. Under ULS conditions, this approach can reduce chain system tension by 23.2 %−64 %, surge and itch by 43 %−44 % and 24 %−41 %, respectively. For the wire mooring system, tension is reduced by 51.5 %−72 %, with surge and pitch decreasing by 48 %−59 % and 19 %−47 %, respectively. Under ALS conditions, this method further reduces drift distance by 60 % and 55 %, showcasing excellent overall performance.

6. Conclusion and outlook

This study focuses on the motion response and mooring line damage issues of FOWT under extreme sea conditions, proposing and verifying the effectiveness of a integrated damping mooring scheme. By integrating Seaflex dampers into various mooring lines (such as chain and wire rope types) and simulating the dynamic behavior of FOWT under 1-year and 50-year return period sea conditions on the OrcaFlex platform, the results show that this scheme can significantly reduce FOWT drift and pitch motion under extreme loading conditions. Additionally, it can maintain better platform posture and safety factors in single point mooring line failure scenarios, providing strong support for the future optimization design and operational safety of FOWT mooring systems. The following is a summary of the main research conclusions:

- The integrated damping mooring technology significantly improves FOWT stability under extreme sea conditions. By integrating Seaflex dampers, the system reduces platform motion and mooring line tension effectively. Under 50-year return period sea states, it decreases surge displacement by 43 %−59 %, pitch angle by 19 %−47 %, and mooring line tension by 23.2 %−72 %.
- Chain and wire rope moorings are particularly effective within this system, reducing horizontal motion by 44 %−58.6 % and further enhancing overall safety under extreme conditions.
- Under accidental limit state (ALS) conditions, the integrated damping system effectively reduces the risk of mooring line failure and maintains reasonable displacement. In single-point mooring line failure scenarios, the integrated damping mooring scheme using chain and wire rope moorings with Seaflex dampers can reduce the platform's maximum drift distance by 55 %−60 %, while also reducing the load spikes caused by line failure, keeping the platform posture within a safe range.

- Seaflex dampers offer broad-spectrum adaptability and lightweight advantages. They perform well across a wide frequency range, reducing platform motion and mooring line tension peaks. Due to their low mass, they do not significantly alter the platform's floating state or increase the mooring load, making them suitable for large-scale FOWT.

Outlook

Based on the above research results, the integrated damping mooring technology offers significant advantages in suppressing FOWT extreme motions and reducing mooring line loads, especially in harsh sea areas with high wind and wave energy. However, certain limitations in this study require further exploration and optimization. Firstly, the integrated damping system requires careful selection of binding locations in practical applications, as different platform structures may significantly influence the optimal binding point. Secondly, local force concentration at the binding points could create potential structural weaknesses, thus requiring reinforcement design to ensure long-term operational safety and reliability. Furthermore, further verification under more complex operating conditions is needed for large-scale wind turbines and varying sea conditions. Future research could focus on the following areas:

(1) To achieve more efficient and stable performance, further optimization of Seaflex damper design parameters, including material properties, structural form, and damping characteristics.

(2) Development of new lightweight, high-strength materials for damper and mooring system manufacturing, thus reducing the overall system load.

(3) Integration of multi-physics field coupling simulations and long-term field tests to assess the system's reliability and economic viability in large-scale commercial deployment.

(4) Exploration of synergetic applications of integrated damping technology with active control, smart materials, and other advanced technologies to enhance floating wind turbines' overall stability and load reduction capacity under extreme sea conditions.

In conclusion, integrated damping mooring technology provides an innovative solution for optimizing the dynamic performance of FOWT. With further design optimization and performance validation, this technology has significant application potential in the future large-scale development of floating wind farms, while also offering more possibilities for addressing operational challenges under extreme sea conditions.

CRediT authorship contribution statement

Haonan Tian: Writing – original draft, Funding acquisition. **Mohsen N. Soltani:** Supervision, Software, Project administration. **Oriol Colomés:** Writing – review & editing, Validation.

Declaration of competing interest

The authors declare that they have no known competing financial interests or personal relationships that could have appeared to influence the work reported in this paper.

Acknowledgement

This paper is supported by a scholarship from the China Scholarship Council under Grant 202207940016.

Data availability

Data will be made available on request.

References

[1] Offshore wind outlook 2019 – analysis. IEA; 2019. https://www.iea.org/reports/offshore-wind-outlook-2019. accessed January 8, 2025.
[2] Alex. global offshore wind report 2024. Global Wind Energy Council; 2024. https://gwec.net/global-offshore-wind-report-2024/. accessed January 8, 2025.
[3] Key aspects of the Paris agreement. UNFCCC; 2025. |n.d. https://unfccc.int/most-requested/key-aspects-of-the-paris-agreement. accessed January 8
[4] Watson S, Moro A, Reis V. Future emerging technologies in the wind power sector: a European perspective. Renew Sustain Energy Rev 2019;113:109270. https://doi.org/10.1016/j.rser.2019.109270.
[5] Zhou B, Zhang Z, Li G, Yang D, Santos M. Review of key technologies for offshore floating wind power generation. Energies 2023;16:710. https://doi.org/10.3390/en16020710.
[6] Khan Afridi S, Ali Koondhar M, Ismail Jamali M, Muhammed Alaas Z, Alsharif MH, Kim M-K, et al. Winds of progress: an in-depth exploration of offshore, floating, and onshore wind turbines as cornerstones for sustainable energy generation and environmental Stewardship. IEEE Access 2024;12:66147–66. https://doi.org/10.1109/ACCESS.2024.3397243.
[7] Yang R, Zheng X, Chen J, Wu Y. Current status and future trends for mooring systems of floating offshore wind turbines. Sustain Mar Struct 2022;4:40–54. https://doi.org/10.36956/sms.v4i2.617.
[8] Zhang Z, Wang X, Zhang X, Zhou C, Wang X. Dynamic responses and mooring line failure analysis of the fully submersible platform for floating wind turbine under typhoon. Eng Struct 2024;301:117334. https://doi.org/10.1016/j.engstruct.2023.117334.
[9] Yang R-Y, Chuang T-C, Zhao C, Johanning L. Dynamic response of an offshore floating wind turbine at accidental limit states—mooring failure event. Appl Sci 2022;12:1525. https://doi.org/10.3390/app12031525.
[10] Grasu G, Liu P. Risk assessment of floating offshore wind turbine. Energy Rep 2023;9:1–18. https://doi.org/10.1016/j.egyr.2022.11.147.

[11] DNV-ST-0437 loads and site conditions for wind turbines. DNV; 2025. n.d. https://www.dnv.com/energy/standards-guidelines/dnv-st-0437-loads-and-site-conditions-for-wind-turbines/. accessed January 8
[12] Robertson A, Jonkman J, Masciola M, Song H, Goupee A, Coulling A, et al. Definition of the semisubmersible floating system for phase ii of OC4. United States: National Renewable Energy Lab. (NREL), Golden, CO; 2014. https://doi.org/10.2172/1155123.
[13] Karimirad M. Modeling aspects of a floating wind turbine for coupled wave–wind-induced dynamic analyses. Renew Energy 2013;53:299–305. https://doi.org/10.1016/j.renene.2012.12.006.
[14] Barrera C, Battistella T, Guanche R, Losada IJ. Mooring system fatigue analysis of a floating offshore wind turbine. Ocean Eng 2020;195:106670. https://doi.org/10.1016/j.oceaneng.2019.106670.
[15] Piscopo V, Scamardella A. Incidence of wind spectrum and turbulence intensity on the design of mooring systems for floating offshore wind turbines. Ocean Eng 2023;290:116377. https://doi.org/10.1016/j.oceaneng.2023.116377.
[16] Chakraborty T, Majumder M. Impact of extreme events on conversion efficiency of wave energy converter. Energy Sci Eng 2020;8:3441–56. https://doi.org/10.1002/ese3.336.
[17] Yeter B, Garbatov Y, Guedes Soares C. Risk-based life-cycle assessment of offshore wind turbine support structures accounting for economic constraints. Struct Saf 2019;81:101867. https://doi.org/10.1016/j.strusafe.2019.06.001.
[18] Li J, Zuo H, Zuo J, Jiang Y, Liu S. Study on the mooring systems attaching clump weights and heavy chains for improving the typhoon resistance of floating offshore wind turbines. Ocean Eng 2024;311:118734. https://doi.org/10.1016/j.oceaneng.2024.118734.
[19] Sheng C, Hong HP. Reliability and fragility assessment of offshore floating wind turbine subjected to tropical cyclone hazard. Struct Saf 2021;93:102138. https://doi.org/10.1016/j.strusafe.2021.102138.
[20] van der Giessen M. Feasibility of mooring system optimization for floating wind turbines in deep water based on static analysis. NTNU; 2021. Master thesis, https://ntnuopen.ntnu.no/ntnu-xmlui/handle/11250/2825805?show=full.
[21] Sumer BM, Kirca VSO. Scour and liquefaction issues for anchors and other subsea structures in floating offshore wind farms: a review. Water Sci Eng 2022;15:3–14. https://doi.org/10.1016/j.wse.2021.11.002.
[22] Moan T, Gao Z, Bachynski EE, Nejad AR. Recent advances in integrated response analysis of floating wind turbines in a reliability perspective. J Offshore Mech Arct Eng 2020;142:052002. https://doi.org/10.1115/1.4046196.
[23] Xu H, Wang L, Zha X, Rui S, Shen K, Guo Z. Dynamic response of floating offshore wind turbine under different stages of typhoon passage. Appl Ocean Res 2024;148:104047. https://doi.org/10.1016/j.apor.2024.104047.
[24] Muskulus M, Hydrodynamics MD. In: Van Kuik G, Peinke J, editors. Soil characteristics and floating wind turbines. Soil characteristics and floating wind turbines, 6. Cham: Springer International Publishing; 2016. p. 67–76. https://doi.org/10.1007/978-3-319-46919-5_8. editors.
[25] Thomsen JB, Bergua R, Jonkman J, Robertson A, Mendoza N, Brown C, et al. Modeling the TETRASPAR floating offshore wind turbine foundation as a flexible structure in OrcaFlex and OpenFAST. Energies 2021;14:7866. https://doi.org/10.3390/en14237866.
[26] Colwell S, Basu B. Tuned liquid column dampers in offshore wind turbines for structural control. Eng Struct 2009;31:358–68. https://doi.org/10.1016/j.engstruct.2008.09.001.
[27] Asfaw AM, Cao L, Ozbulut OE, Ricles J. Development of a shape memory alloy-based friction damper and its experimental characterization considering rate and temperature effects. Eng Struct 2022;273:115101. https://doi.org/10.1016/j.engstruct.2022.115101.
[28] Borg M, Shires A, Collu M. Offshore floating vertical axis wind turbines, dynamics modelling state of the art. part I: aerodynamics. Renew Sustain Energy Rev 2014;39:1214–25. https://doi.org/10.1016/j.rser.2014.07.096.
[29] Tian H, Soltani MN, Colomés O. Enhancing floating wind turbine reliability with integrated damping mooring. In: 2024 13th International conference on renewable energy research and applications (ICRERA); 2024. p. 523–30. https://doi.org/10.1109/ICRERA62673.2024.10815222.
[30] IEC 61400-3-1:2019 - Wind energy generation systems - Part 3-1: design requirements for fixed offshore wind turbines. ITeh Standards n.d. https://standards.iteh.ai/catalog/standards/iec/4aa2c08f-8fc5-48bf-b968-bf04539816a5/iec-61400-3-1-2019.
[31] Rushikesh K, Vijay KG, Kumar GV, Venugopal V. Coupled response analysis of a floating wind turbine with free hanging solid ballast. J Ocean Eng Mar Energy 2024;10:749–72. https://doi.org/10.1007/s40722-024-00343-z.
[32] Thies PR, Johanning L, McEvoy P. A novel mooring tether for peak load mitigation: initial performance and service simulation testing. Int J Mar Energy 2014;7:43–56. https://doi.org/10.1016/j.ijome.2014.06.001.
[33] Zhao Z, Li X, Wang W, Shi W. Analysis of dynamic characteristics of an ultra-large semi-submersible floating wind turbine. J Mar Sci Eng 2019;7:169. https://doi.org/10.3390/jmse7060169.
[34] Benassai G, Campanile A, Piscopo V, Scamardella A. Ultimate and accidental limit state design for mooring systems of floating offshore wind turbines. Ocean Eng 2014;92:64–74. https://doi.org/10.1016/j.oceaneng.2014.09.036.
[35] Ochi MK. Ocean waves: the stochastic approach. Cambridge, U.K, New York: Cambridge University Press; 1998.
[36] Tian H, Soltani MN, Colomés O. Enhancing floating wind turbine reliability with integrated damping mooring. In: 2024 13th International Conference on renewable energy research and applications (ICRERA); 2024. p. 523–30. https://doi.org/10.1109/ICRERA62673.2024.10815222.
[37] A VA, Robertson MJ. Comparison of OrcaFlex and OpenFAST for offshore wind turbine analysis. J Wind Eng Ind Aerodyn 2014;127:175–88.
[38] DNV-RP-0286 coupled analysis of floating wind turbines. DNV; 2025. n.d. https://www.dnv.com/energy/standards-guidelines/dnv-rp-0286-coupled-analysis-of-floating-wind-turbines/. accessed January 13
[39] Jonkman J, Butterfield S, Musial W, Scott G. Definition of a 5-mw reference wind turbine for offshore system development. Syst Dev 2009.
[40] DNVGL-OS-E301 - Position Mooring. GlobalSpec; 2025. |n.d. https://standards.globalspec.com/std/9956378/dnvgl-os-e301. accessed January 13
[41] Neisi A, Ghassemi H, Iranmanesh M, He G. Effect of the multi-segment mooring system by buoy and clump weights on the dynamic motions of the floating platform. Ocean Eng 2022;260:111990. https://doi.org/10.1016/j.oceaneng.2022.111990.
[42] Huo F, Xu J, Yang H, Yuan Z, Shen Z. Study on characteristics of mooring system of a new floating offshore wind turbine in shallow water by experiment. Front Energy Res 2023;10:1007996. https://doi.org/10.3389/fenrg.2022.1007996.
[43] Lozon E, Hall M, McEvoy P, Kim S, Ling B. Design and analysis of a floating-wind shallow-water mooring system featuring polymer springs: preprint. Renew Energy 2022.
[44] Liu B, Yu J. Dynamic response and mooring fracture performance analysis of a semi-submersible floating offshore wind turbine under freak waves. J Mar Sci Eng 2024;12:1414. https://doi.org/10.3390/jmse12081414.